Journal of Hydrology 630 (2024) 130770

Contents lists available at ScienceDirect

Journal of Hydrology

journal homepage: www.elsevier.com/locate/jhydrol

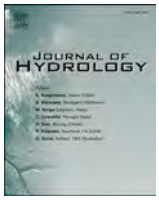

Research papers

Control of soil mantle thickness and land cover types on groundwater recharge of karst aquifers in Mediterranean areas

Delia Cusano [a,*], Daniele Lepore [a], Vincenzo Allocca [a], Pantaleone De Vita [a]

[a] Department of Earth, Environmental and Resources Sciences (DiSTAR), University of Naples Federico II, Italy

ARTICLE INFO

Keywords:
Karst aquifers
Soil mantle
Groundwater recharge
Evapotranspiration
Southern Apennines

ABSTRACT

Karst aquifers represent the fundamental groundwater resources in Italy and in many other countries because supplying urban areas of drinking water and sustaining industrial and agricultural activities. Accordingly, advancing the assessment of groundwater recharge of these aquifers is a major scientific challenge, specifically if considering the hydrological role exerted by soil covering and the related land cover types. In such a framework, the soil water balance model is an effective tool for providing accurate estimates of groundwater recharge depending on precise field and laboratory characterizations of the soil covering.

Considering the features of karst aquifers of southern Italy and the ubiquitous occurrence of a soil mantle, mainly of ash-fall pyroclastic origin, a methodology based on field and laboratory characterizations, as well as modeling approaches, is proposed in this work to advance the knowledge on groundwater recharge processes. The experimental approach was applied to the Soprano-Vesole-Chianello Mts. karst aquifer (Campania region, southern Italy) which is considered representative of karst aquifers of southern Italy and Mediterranean areas as well.

A comprehensive characterization of the soil mantle was developed, considering different land cover classes, measurements and stochastic spatial modeling of soil thickness. The unsaturated hydraulic properties of undisturbed soil samples were analyzed by laboratory tests resulting in the determination of Soil Water Retention Curves (SWRCs). Moreover, a field monitoring of soil water content was carried out by multi-profile soil moisture sensors, allowing the assessment of the hydrological response of the soil covering and of the regime of groundwater recharge process as well.

Among the principal outcomes is the recognition, for each land cover class, of different values of the depth to which the evapotranspiration effect is extended. Based on a consistent spatial modeling of soil thickness and soil hydrologic properties, the Soil Water Balance code (SWB 1.2) was applied to evaluate the spatial and temporal variability of the groundwater recharge of the karst aquifer.

As a principal outcome, groundwater recharge rates were found to be dependent on land cover class and soil thickness as well, showing lower values for wooded areas and higher for denudated ones, respectively due to the higher and lower evapotranspiration rates.

1. Introduction

Karst aquifers are considered worldwide an important source of water supply for all human uses and for the equilibrium of fluvial ecosystems. Groundwater resources of the Mediterranean karst aquifers have been considered relevant since the development of ancient settlements whose foundation was strictly reliant on the occurrence of huge springs (Bakalowicz, 2005). 40 karst aquifers, covering about 44 % of the whole territory (8560 km^2) and forming the principal mountain ranges, were recognized in a large sector of southern Italy (Allocca et al., 2014; De Vita et al., 2018; Ruggieri et al., 2021). These aquifers play a vital role in the socio-economic development of the territory and in sustaining the groundwater-dependent ecosystems (Goldscheider, 2015; Hartmann et al., 2014). Nowadays, a progressive degradation of the groundwater quality, due to groundwater overexploitation and pollution phenomena, has been noticed especially in karst aquifers adjoining to the main urban areas (Cusano et al., 2019; Tufano et al., 2020). Furthermore, the effects of climate change, such as the decreasing trend

* Corresponding author.
E-mail addresses: delia.cusano@unina.it (D. Cusano), daniele.lepore@unina.it (D. Lepore), vincenzo.allocca@unina.it (V. Allocca), padevita@unina.it (P. De Vita).

https://doi.org/10.1016/j.jhydrol.2024.130770
Received 31 August 2023; Received in revised form 15 December 2023; Accepted 29 December 2023
Available online 26 January 2024

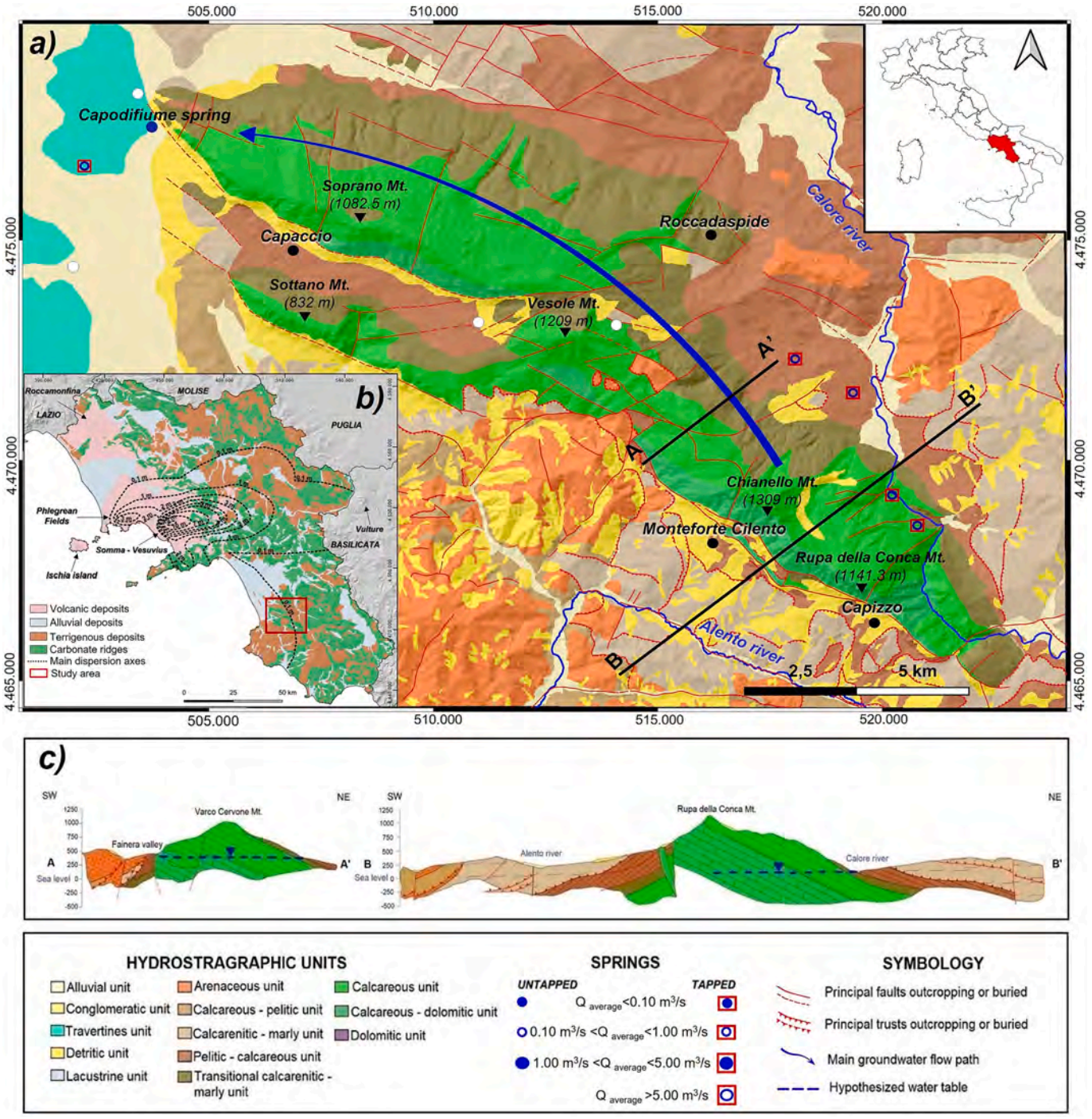

Fig. 1. A) hydrogeological map of Soprano-Vesole-Chianello Mts. karst aquifer. coordinate system utm wgs 84, 33 N zone; b) Total thickness (isopach) map of ash-fall deposits in Campania region, excerpt from Celico and Guadagno (1998) and Bisson et al. (2007). c) Hydrogeological cross-sections.

of annual precipitation and the increasing of air temperature represent a threat for the availability of groundwater resources in North America and Europe (Christensen et al., 2007) and southern Italy as well (Polemio and Casarano, 2008). In order to properly manage the groundwater resources avoiding overexploitation, the correct estimation of groundwater recharge processes at various space-time scales as well as the assessment of the hydrological forcing controlling these processes represent key aspects to be understood. The hydrogeological and geomorphological heterogeneity of karst aquifers make the estimation of groundwater recharge and its spatial variability, a challenging issue within the hydrological studies aimed at quantifying the present and future groundwater availability (Hartmann et al., 2014).

It is known that the groundwater recharge depends on many factors such as climate, land use and land cover, geology, soil texture and structure, among the others. Specifically, in vadose zone studies, groundwater recharge is synonymously used for effective infiltration, percolation or residual flux to connote water movement below the rooting zone toward the groundwater zone (Scanlon et al., 2002).

Generally, the hydrological processes occurring in the vadose zone of karst aquifers have been poorly investigated, especially considering the hydrological role exerted by the soil covering. Considering the peculiar covering of karst aquifers of southern Italy with ash-fall pyroclastic soils

erupted, starting from Pleistocene, by volcanic centers of Campania (Roccamonfina, Ischia Island, Phlegrean Fields and Somma-Vesuvius) and Basilicata regions (Vulture) (Fig. 1b), it is fundamental to characterize and model the groundwater recharge processes depending on the hydrological behavior of the soil covering and of the related land cover types. Specifically, given their high-water retention capacity (Fusco et al., 2017), ash-fall pyroclastic soils play an important role in the soil water balance and on groundwater recharge process as well. Therefore, the soil hydrological properties and its antecedent moisture conditions (Charlier et al., 2012; Fu et al., 2016; Trček, 2007) have to be considered because controlling the infiltration rate and the storage capacity of water.

The influence of the soil covering on groundwater recharge has been already investigated for different environments (Mao and Cherkauer, 2009; Nosetto et al., 2012) and at various spatial scales, from local to global. In all of them, observed and experimental data have shown the role of vegetation types on runoff initiation and soil moisture storage (Kovačič et al., 2020; Zhang et al., 2019). In particular, the deep-rooted vegetation was recognized reducing the groundwater recharge (Matheussen et al., 2000), due to the higher losses from evapotranspiration phenomena, compared to shallow-rooted vegetation (Pinto et al., 2014).

Recently, (Jukić et al., 2021) introduced a new method for the estimation of groundwater recharge in karst environments based on partial cross-correlation method (PMC) applied to time series of precipitation, air temperature, relative humidity and spring discharge as well as on a simple conceptual model of water balance of the soil cover. Results were compared with those obtained by other different empirical models (Borzì et al., 2020; Santoro, 1970; Srebrenović, 1986; Turc, 1954; Žugaj, 1995).

However, these studies have not yet focused the joint role of the thickness of the soil covering and the land cover type on groundwater recharge processes. Consequently, the hydrological behavior and regime of unsaturated soil mantle represents a novel scientific challenge in the hydrogeology field and an important advance for modeling groundwater recharge of karst aquifers and its spatial variability. In such a framework, studies carried out in the last decades on carbonate mountains of southern Apennines have prepared the knowledge bases by considering the hydrological behavior of ash-fall pyroclastic soil covering leading to slope instabilities (De Vita et al., 2018; Del Soldato et al., 2018).

In this work a methodology based on field, laboratory activities and modeling approaches, allowed to advance the knowledge regarding the hydrological role of the soil mantle on the recharge processes of the karst aquifers. The Soprano-Vesole-Chianello Mts. karst aquifer was identified as a representative test area due to its hydrogeological and land cover

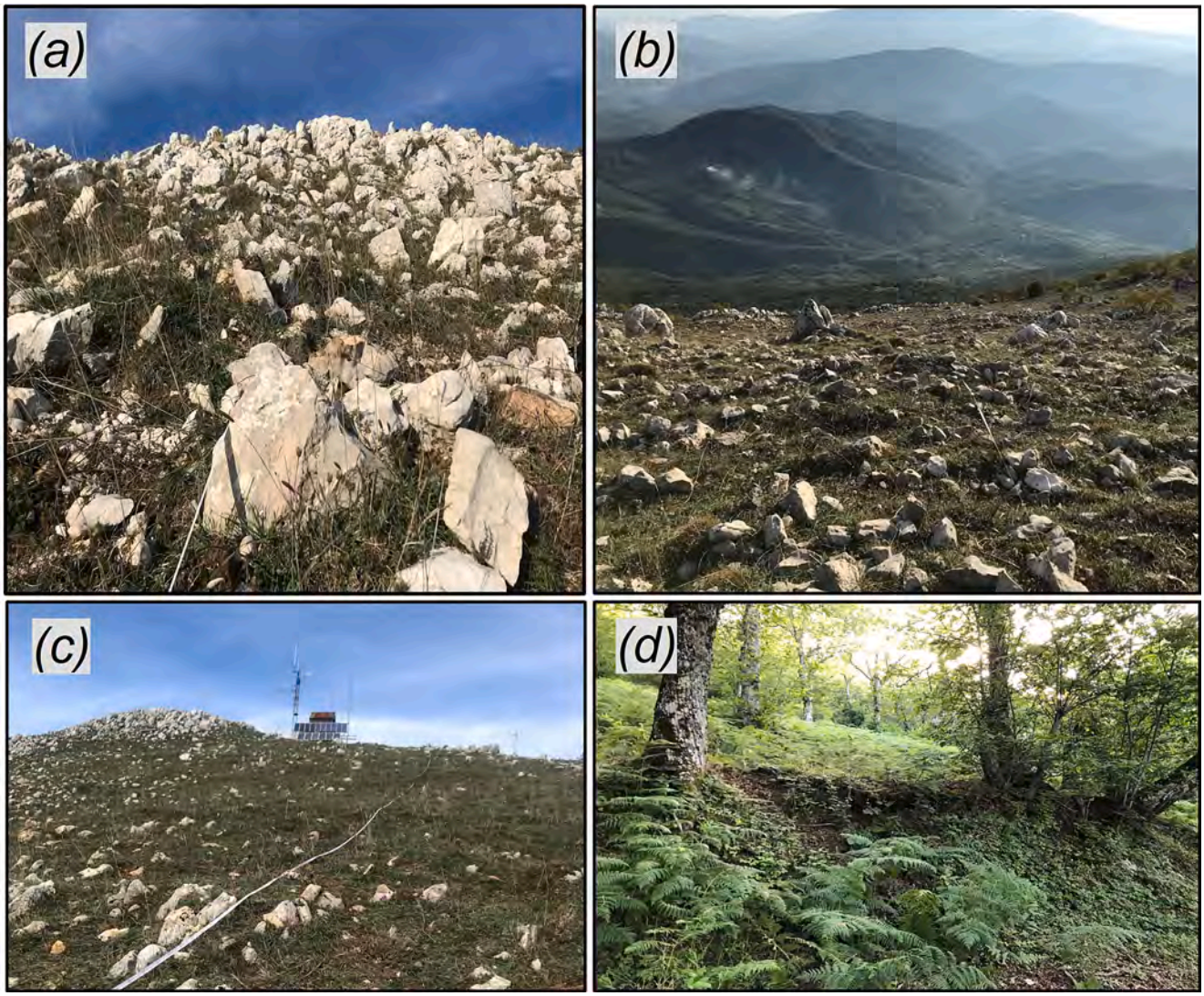

Fig. 2. Land cover classes identified in the study area: a) denudated areas with prevailing outcropping rocks, erratic and isolated thin soil pockets covered by scarce grassy vegetation; b) denudated areas with sparse outcropping rocks, discontinuous and connected soil pockets and grassy vegetation; c) areas with continuous and thicker soil covering and grassland; d) areas with the thickest and continuous soil covering and wooded vegetation.

Table 1
Location, land cover class, sampling depth and pedologic soil horizon of undisturbed and disturbed soil samples (*).

Sampling location	Land cover class	Sampling depth (m)	Pedologic soil horizon	Undisturbed soil samples ID	No. of undisturbed soil samples	Disturbed soil samples ID	No. of disturbed soil samples
Chianello Mt.	Class c	0.30	B	I	4	I*	1
Capizzo	Class d	0.30	B	II	2	II*	1
		0.70			2	III*	1
		1.20	Bb (paleosol)	III	2	IV*	1

features. Objectives of this study are: (i) field recognitions and modeling of soil thickness and land cover types; (ii) characterization of unsaturated/saturated soil hydraulic properties; (iii) meteorological and soil hydrological monitoring across the recharge catchment to characterize variables controlling the evapotranspiration processes; and (iv) groundwater recharge estimates calculated by the Soil Water Balance code (Westenbroek et al., 2010).

2. Geological and hydrogeological settings

The studied area is in the Cilento subregion (Campania, southern Italy) and characterized by the outcrop of a sector of the Apennine carbonate platform unit (Vitale et al., 2012) corresponding to the Soprano-Vesole-Chianello Mts. ridge. This mountain ridge extends WNW – ESE and separates the Calore river valley to the north from the Alento valley to the south. The Chianello Mt. ridge (1309 m a.s.l.) represents the major height, while the Vesole Mt. (1209 m a.s.l.) and the Soprano Mt. (1082.5 m a.s.l.) the minor ones. The mountain ridge is formed by the tectonic unit of the Meso-Cenozoic carbonate platform domain (more than 1300 m thick) constituted by (a) dolomitic series (late Triassic), (b) limestone and dolomitic limestone (Jurassic-Cretaceous), (c) calcareous breccia and marls (Paleocene-Eocene), (d) bioclastic grainstones (Aquitanian-Burdigalian). The carbonate unit is tectonically over-thrust by turbidite and deep-basin terrigenous deposits of the "Internal Units" cropping out at lower altitudes in the adjoining Calore and Alento river valleys and forming gentle hilly morphology. From a structural point of view, the Soprano-Vesole-Chianello ridge is shaped by a NE dipping forelimb of a regional anticline whose backlimb is down faulted to the SW (Vitale et al., 2012). The series is also dislocated by a pattern of *meso*-faults, NW-SE and NE-SW oriented (Torrente et al., 2000). For these structural features, the Paleocene series outcrop only along the northern slopes of the ridge (Simone et al., 2012).

From a hydrogeological point of view, the Soprano-Vesole-Chianello Mts. carbonate ridge can be considered one of the main representative karst aquifers of the southern Italy and the Mediterranean area as well. Outcrops of carbonate rocks are extended for this aquifer over 75.35 km^2 (Fig. 1a). The complex stratigraphic and structural settings play an important control on groundwater circulation. The carbonate outcrops are characterized by high permeability grade due to fracturing and karst and by a lateral confinement with low-permeability terrigenous series that limit and constrain the groundwater flow towards the main outlet represented by the Capodifiume spring (27 m a.s.l.), with a mean annual discharge of about 3.0 m^3/s (Fig. 1a and 1b) (Celico, 1983; De Vita et al., 2018). The basal groundwater circulation scheme has a flow direction oriented from SE to NW (Fig. 1a), feeding also other minor springs located in the Paestum Plain with low altitude (35 m a.s.l.) which are characterized by a high mineralization.

As the other karst aquifers of southern Italy, the studied one is characterized by the covering of an ash-fall pyroclastic soil mantle, whose spatial continuity, thickness and stratigraphic settings depend on the distance from the Somma-Vesuvius and Phlegrean Fields volcanoes, orientation of dispersal axes (Fig. 1b) and denudational processes. Despite the relevant distance of the study area from these volcanic centers (about 100 km), ash-fall pyroclastic soils were recognized as being significant and associated to specific land cover classes.

The climate of the studied karst aquifer varies from the Mediterranean type (Csa) in the coastal area (up to 600 m a.s.l.) to the Mediterranean mild climate (Csb) in the inland areas (widespread at altitude above 600–800 m a.s.l.) (Beck et al., 2018), with a mean annual rainfall of about 1250 $mm \cdot y^{-1}$ and mean annual air temperature of about 11 °C.

3. Data and methods

3.1. Spatial modeling of soil mantle and land cover

With the aim to understand the hydrological role of the soil mantle on groundwater recharge, a detailed characterization of the surficial hydrogeological system formed by soils mantling the carbonate bedrock was carried out.

The Soprano-Vesole-Chianello Mts. carbonate ridge is characterized by geomorphological settings and variability of soil cover and vegetation types which are typical of Mediterranean carbonate mountains. The stratigraphic surveys of soil mantle by test pits, aimed at the acquisition of detailed stratigraphic data, allowed to recognize the lithostratigraphic and pedologic soil horizons (USDA, 1987) as well as to measure the soil thickness. Specifically, the measurement of soil thickness was carried out for different land cover types by the nailing of a steel rod along 17 straight transects with length varying from 20 m to 50 m, depending on the land cover types and local logistic conditions, and with a spacing ranging from 0.20 m to 1.00 m. A total of 1435 soil thickness data were collected and analyzed by a probabilistic analysis to assess the spatial variability depending on the land cover type. Based on field observations, including spatial continuity and thickness of soil mantle as well as vegetation types, four land cover classes were recognized: (a) denudated areas with prevailing outcropping rocks, (b) denudated areas with discontinuous soil pockets, (c) denudated areas with continuous soil and d) wooded areas (Fig. 2).

Moreover, a detailed land cover map of the study karst aquifer was reconstructed on the basis of field observations and a supervised classification technique of high resolution Google Earth orthophotos (0.70 m × 0.70 m resolution), carried out by the SCP plugin (Congedo, 2016) working in the QGIS platform. At this scope, 155 rectangular adjoining images (800 m × 1280 m) were gathered, georeferenced and joined to create a unique framework map of the studied karst aquifer. The images were progressively aligned, georeferenced and juxtaposed sequentially.

In order to model spatially the thickness of the soil mantle, a probabilistic model based on the Gamma distribution Eq. (1) was applied to soil thickness data to obtain a stochastic soil thickness map for each land cover class, with a spatial resolution of 10 m × 10 m. Specifically, by the Eq. (1), stochastic values (f(x)) characterized by a statistical distribution comparable to that of sampled values, were generated.

$$f_{k,\theta}(x) = \frac{x^{k-1} \bullet e^{-\frac{x}{\theta}}}{\theta^k \bullet \Gamma(k)}; x > 0 \text{ and } k,\ \theta > 0 \quad (1)$$

Where f(x) represents the probability density function, k is the shape parameter, θ is the scale parameter and (k) is the gamma function defined by the Eq. (2):

$$\Gamma(k) = \int_0^{\infty} x^{k-1} \bullet e^{-x} \bullet dx \quad (2)$$

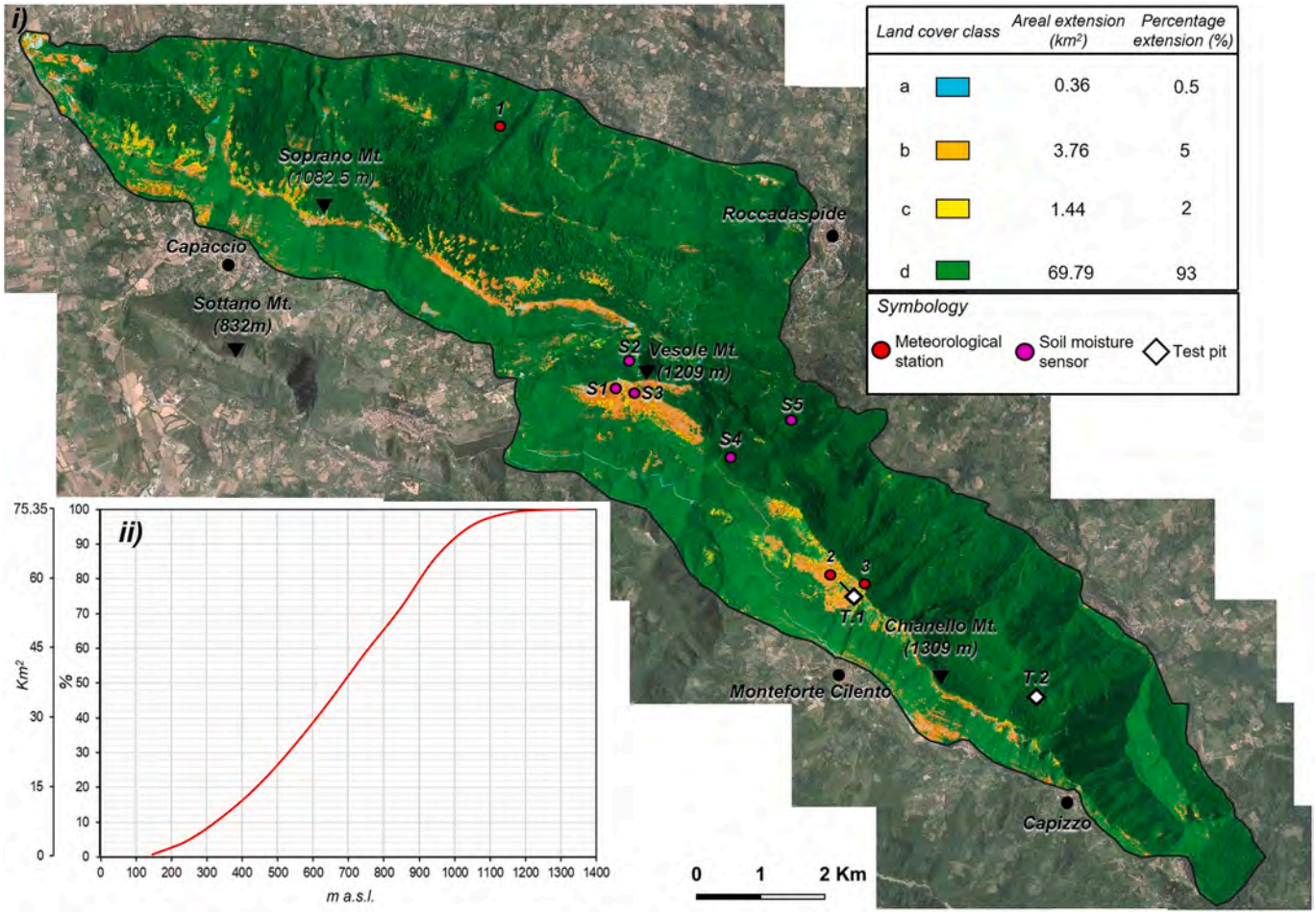

Fig. 3. I) land cover map of Soprano-Vesole-Chianello Mts. karst aquifer. keys to symbols. location of meteorological stations: 1. soprano mt. (636 m a.s.l.); 2. middle-upper southwestern slope of the Chianello Mt. (1022 m a.s.l.); 3. Mt. Chianello top (1309 m a.s.l.). Location of soil moisture sensors: S2, S4 and S5 with a length of 1.0 m: S1 and S3 with a length of 0.40 m. Location of test pits: T1 and T2. ii) Hypsometric curve of the study aquifer.

3.2. Characterization of physical and index properties of soil mantle

10 undisturbed and 4 disturbed soil samples were collected for laboratory characterization of physical and hydrologic properties (Table 1). Undisturbed soil samples were collected into test pits by the gently pushing of brass cylinders (60 mm diameter) into the soil at the wanted depth, while disturbed samples by the collection of reworked soil by a shovel.

Physical properties of undisturbed soil samples, depending on relationships between volume and weight, were determined by laboratory tests. The natural unit weight (γ) and dry unit weight (γ_{dry}) were determined by a standard procedure (British Standard – BS 1377, 1990) based on the known volume of the sampler cylinder (344.48 cm^3) and the weighings in natural condition and after ovendrying, respectively. Index properties were determined on disturbed soil samples. Specifically, the specific gravity of solid particles (G_s), the Atterberg limits, liquid (w_L) and plastic (w_P) limits as well as the organic matter content were determined by standard procedures (ASTM D854-83, 1983; ASTM D4318, 1984; ASTM-D2974, 2000). Subsequently the porosity (n) was calculated by the Eq. (3):

$$n = 1 - \frac{\gamma_{dry}}{G_s} \tag{3}$$

The grain size analysis, by means of sieving (ASTM D421-85, 1998) and sedimentation techniques (ASTM D422-63, 1998), were also determined. Results allowed to apply USDA (USDA, 1987) and USCS (Casagrande, 1948) classifications.

The undisturbed soil samples were also used for the estimation of unsaturated/saturated soil properties (paragraph 3.3).

3.3. Unsaturated and saturated hydraulic characterization of soil mantle

The unsaturated hydraulic properties of soils were determined by the reconstruction of Soil Water Retention Curves (SWRCs) with the Tempe Pressure Cell apparatus (Soilmoisture Inc.). The SWRCs were determined by the simultaneous testing of sets of four undisturbed soil samples, collected for the same soil horizon at the wanted depth (Table 1). After the closure in an assembly made by caps of plastic material provided by a vent and a porous plate at the base, the undisturbed samples were saturated by a partial submersion in free water and then tested with a series of increasing air pressure steps ranging from 0.01 to 1 bar. The procedure consisted in the application of an air pressure value, regulated at the established value, to the assembly containing the soil sample, thus allowing the drainage of the capillary water through the porous plate. The reaching of the equilibrium between the air pressure applied and the menisci forces was monitored by the observation of the end of water outflow. Subsequently, by the oven-drying of soil samples, the residual and saturation water contents (θ_r and θ_s) were estimated and, finally, from each dry weight measurement, the volumetric water content (θ) was calculated. From these data, optimized values of parameters of the van Genuchten equation (van Genuchten, 1980) describing SWRC Eq. (4) were obtained by means of RETC code (van Genuchten et al., 1991).

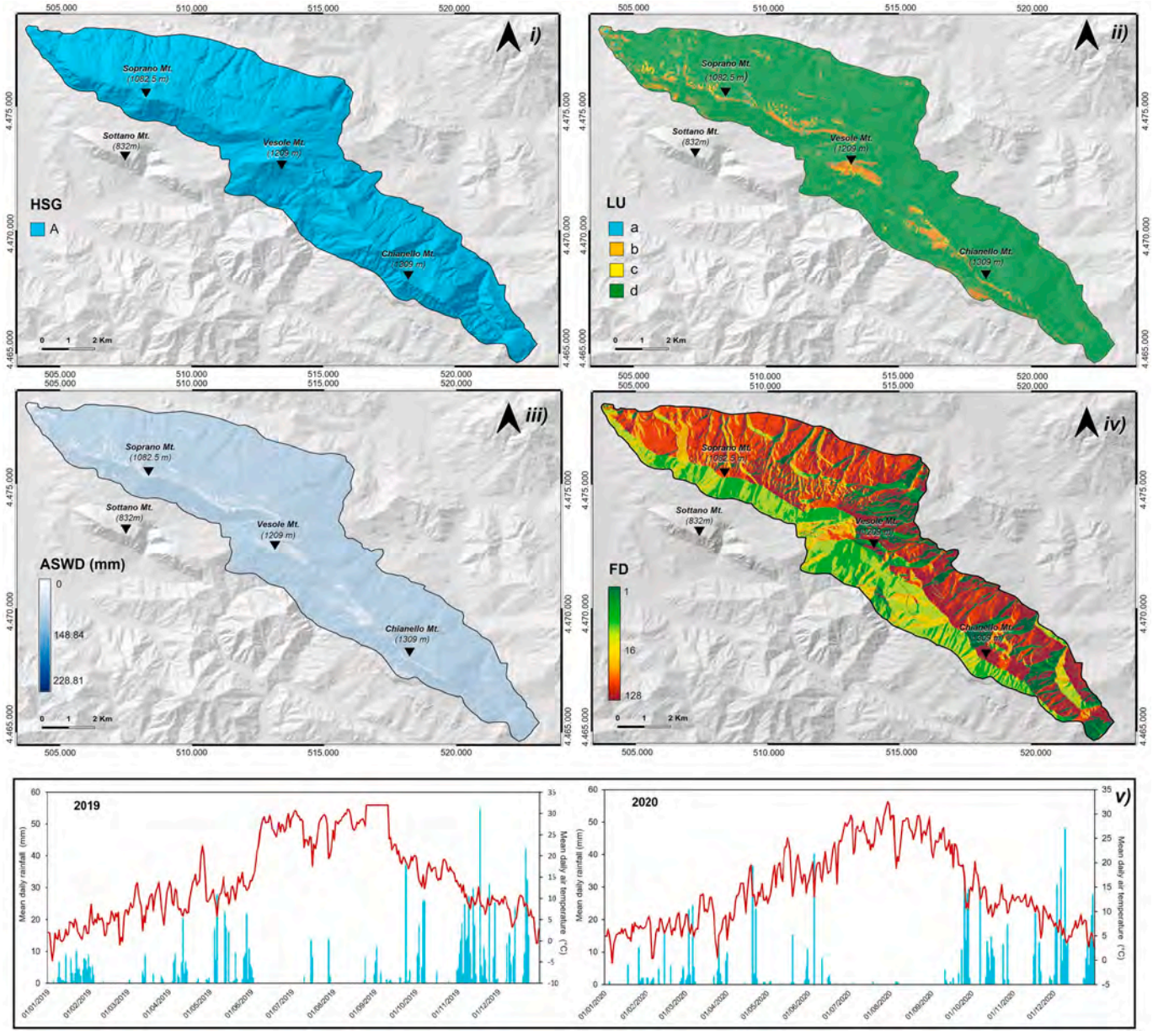

Fig. 4. Data required for the application of the SWB code. Gridded data layer: i) Hydrologic Soil Group (HSG) map; ii) Land Use (LU) map; iii) Available Soil Water Depth (ASWD) map; iv) Flow Direction (FD) map; v) rainfall and air temperature time series.

$$\theta(h) = \theta r + \frac{\theta s - \theta r}{[1 + |\alpha/|h|^n]^m} \quad (4)$$

where, θs ($m^3 \bullet m^{-3}$) is the saturated volumetric water content, θr ($m^3 \bullet m^{-3}$) the residual volumetric water content, h (m) is soil matrix pressure head, α (m^{-1}) is the inverse of the air-entry head, n (dimensionless) is the pore-size distribution parameter, and m = 1–1/n.

Based on the estimation of SWRCs, the Available Soil Water Capacity (ASWC) and Available Soil Water Depth (ASWD) were calculated by using the following equations Eqs. (5) and (6):

$$\text{ASWC } (\%) = \theta_{FC} - \theta_{PWP} \quad (5)$$

$$\text{ASWD (mm)} = (\theta_{FC} - \theta_{PWP}) \times h \quad (6)$$

where, ASWC represents the Available Soil Water Capacity, θ_{FC} is the soil water content at Field Capacity (FC), θ_{PWP} is the soil water content at Permanent Wilting Point (PWP) and h represents the root-zone depth (mm) corresponding to the evapotranspiration zone.

Moreover, the saturated hydraulic conductivity K_{sat}, considered as a key input to model and simulate groundwater flow, was calculated by the Saxton pedotransfer function (Bouma, 1989; Saxton et al., 1986) Eq. (7), which was developed to estimate K_{sat} from the relative amount of sand and clay as well as the porosity value.

$$\text{Ksat} = \exp\left[12.01 - 0.0755 \bullet \%\,\text{SA} + \left(-3.895 + 0.03671 \bullet \%\,\text{SA} - 0.1103 \bullet \%\,\text{CL} + 0.00087546 \bullet \%\,\text{CL}^2\right)/\text{n}\right] \quad (7)$$

where, SA is sand (%), CL is clay (%) and n is porosity.

3.4. Field hydrological monitoring of the soil mantle

Field monitoring of soil water content by means of multi-profile soil moisture sensors (Dataflow System Inc.) was carried out in order to assess the hydrological regime of the soil mantle and its control on groundwater recharge process. The multi-profile soil moisture logger adopted measures both the soil moisture and temperature at multiple

(up to 5) discrete points along the length of a rod with a sensor spacings varying from 0.20 m to 0.10 m. In total, five measuring verticals, namely rod with sensors, were installed in test sites representative of different land cover classes. Three measuring verticals, with a length of 1.0 m and five soil moisture sensors, located at depths of 0.10, 0.20, 0.40, 0.60, 1.00 m (S2, S4 and S5, Fig. 3), were installed in wooded areas (class d), instead two measuring verticals, with a length of 0.40 m and three soil moisture sensors, located at depths of 0.10, 0.30 and 0.40 m (S1 and S3, Fig. 3), were installed in c and b land cover classes respectively. The class a was not considered due the prevailing outcrop of the bedrock.

The monitoring period was comprised between January 2021 and June 2022 while the measurement frequency was set with a periodicity of 30 min. Soil moisture data were analyzed jointly to daily rainfall data, gathered by three meteorological stations which were installed in the studied area: one at Soprano Mt. (1, Fig. 3, 636 m a.s.l.) and the other two at the middle-upper southwestern slope of the Chianello Mt. (2, Fig. 3, 1022 m a.s.l.) and at its top (3, Fig. 3, 1309 m a.s.l.). Considering the altitude of meteorological stations, which are included in the altitude range of carbonate mountain ridge, the rainfall mean values were considered representative for the entire study area, and used both for the correlation with soil moisture data and as input climatological data of the Soil Water Balance model.

3.5. Soil water balance (SWB, 1.2)

For this study, the Soil Water Balance code (SWB 1.2, Westenbroek et al., 2010) developed by USGS, was applied to calculate spatial and temporal variations of groundwater recharge and evapotranspiration considering the different land cover classes, for the 2019 and 2020. The code, based on a modified Thornthwaite and Mather (1957) soil water balance approach, estimates the recharge by geographic system data layers in combination with tabular climatological data.

The SWB code is based on a mass balance equation, calculated at daily time step Eq. (8):

$$\text{Recharge} = (\text{precip} + \text{snowmelt} + \text{inflow}) - (\text{interception} + \text{outflow} + \text{ET}) - \triangle_{\text{soil moisture}} \quad (8)$$

where precip ($mm{\cdot}day^{-1}$) are precipitations, snowmelt ($mm{\cdot}day^{-1}$) is calculated by the daily mean, maximum and minimum air temperatures, inflow ($mm{\cdot}day^{-1}$) is calculated by the use of a flow-direction grid derived from a Digital Elevation Model (DEM) to estimate outflow (surface runoff) to adjoining downslope grid cells, interception ($mm{\cdot}day^{-1}$) represents the amount of rainfall used by vegetation and evaporated or transpired from plant surface (Westenbroek et al., 2010), outflow or surface runoff ($mm{\cdot}day^{-1}$). The latter is calculated by the curve number rainfall-runoff relationship (Cronshey, 1986), proposed by U.S. Department of Agriculture, Natural Resources Conservation Service (NRCS). ET ($mm{\cdot}day^{-1}$) is the evapotranspiration, calculated with the Thornthwaite–Mather method and $\triangle_{\text{soil moisture}}$ ($mm{\cdot}day^{-1}$) represents the variation in soil moisture. Following, the groundwater recharge is estimated by a distributed approach by the SWB code as deep percolation and represents the excess water in the root zone of the soil column, which do not contribute to evapotranspiration nor to runoff. Excess water is calculated by subtracting the sum of the outputs (evapotranspiration, surface runoff and interception) from the inputs (precipitation, snowmelt and surface runoff from adjoining cells) (Verma et al., 2017). Given the high hydraulic conductivity of the studied carbonate bedrock at the base of soil mantle as well as in the rest of the very extended unsaturated zone, the effective infiltration resulting from the water balance of the soil column was considered properly as groundwater recharge of the underlying karst aquifer.

The SWB code requires four types of gridded data layers, elaborated in a GIS environment with a spatial resolution of 10 m × 10 m, corresponding to:

- Hydrologic Soil Group map (**HSG**): ASCII integer grid with values equal to 1, corresponding to soil group A according to the U.S. Department of Agriculture, Natural Resources Conservation Service (National Research Council, 2001). This value was recognized for the whole study area, based on field observations, laboratory testing and estimation of K_{sat}, corresponding to an infiltration rate >0.3 in.·h^{-1} (>7.6 mm·h^{-1}; >2.11×10^{-6} m·s^{-1}) (Fig. 4i).
- Land Use map (**LU**): ASCII file containing integer values for each grid cell in the model domain, assigned to describe the land cover types. The land cover map of Soprano – Vesole – Chianello Mts. karst aquifer was used as LU map (LU, Fig. 4ii).
- Available Soil Water Depth map (**ASWD**): ASCII file contains real number values for each grid cell in the model domain. Considering the results of the spatial modeling of soil thickness and characterization of Field Capacity (θ_{FC}) and Wilting Point (θ_{WP}), the stochastic map of Available Soil Water Depth (ASWD) was reconstructed and implemented in the SWB code (Fig. 4iii).
- Flow Direction map (**FD**): ASCII grid of surface water flow direction obtained by using the ArcGIS D8 algorithm, from a DEM (10 m × 10 m spatial resolution) (Fig. 4iv).

Finally, tabular climate data for 2019 and 2020 were implemented in the SWB model: daily rainfall (mm) and mean air temperature (°C), gathered from three meteorological stations were considered as meteorological input. In this way, mean annual cumulative precipitation of 2019 and 2020 were estimated equal to 1102.8 and 927.2 mm respectively, while the mean air temperature was estimated equal to 14.7 °C for both years (Fig. 4v).

To assess and validate the performance of the SWB code, the modeling results were compared with the results of the Thornthwaite-Mather soil water balance method (1957) in terms of evapotranspiration rates.

The Thornthwaite-Mather method is an empirical approach used for estimating monthly water balance. This method provides a quantification of the available water content in the soil and allows to estimate the actual evapotranspiration (AET). The soil water balance is calculated by latitude, average monthly temperature, precipitation values and soil water content. These variables are used to calculate the potential evapotranspiration (PET), the actual evapotranspiration (AET) and the Available Soil Water Depth (ASWD). The Eq. (9) has been proposed by Thornthwaite, (1955) to obtain the potential evapotranspiration (PET):

$$\text{PET} = \sum_{i=1}^{12} k \times \left[1.6 \times \left(\frac{T_i}{I}\right)^{\alpha}\right] \quad (9)$$

where PET is the potential evapotranspiration (mm), k is a coefficient that depends on the monthly average of hours of insolation and function of the latitude and month, T_i is the mean monthly air temperature (°C) for the i^{th} month, I is the annual thermal index that is given by the sum of the monthly thermal indexes, where α is expressed by Eq. (10):

$$\alpha = (675 \times 10^{-9} \cdot I^3 - 771 \times 10^{-7} \cdot I^2) + (1792 \times 10^{-5} \cdot I + 0.49239) \quad (10)$$

3.6. Estimation of empirical coefficients of groundwater recharge

In order to express results of soil water balance assessment in terms of empirical approaches based on coefficients linking precipitation to groundwater recharge, the Effective Infiltration Coefficient (EIC, %; Bonacci, 2001; Drogue, 1971), which incorporates the complex processes existing in the vadose zone (evapotranspiration and percolation phenomena), was estimated by applying the Eq. (11):

$$\text{EIC} = \frac{Ie}{P} \quad (11)$$

where, Ie is effective infiltration (mm) and P (mm) is rainfall.

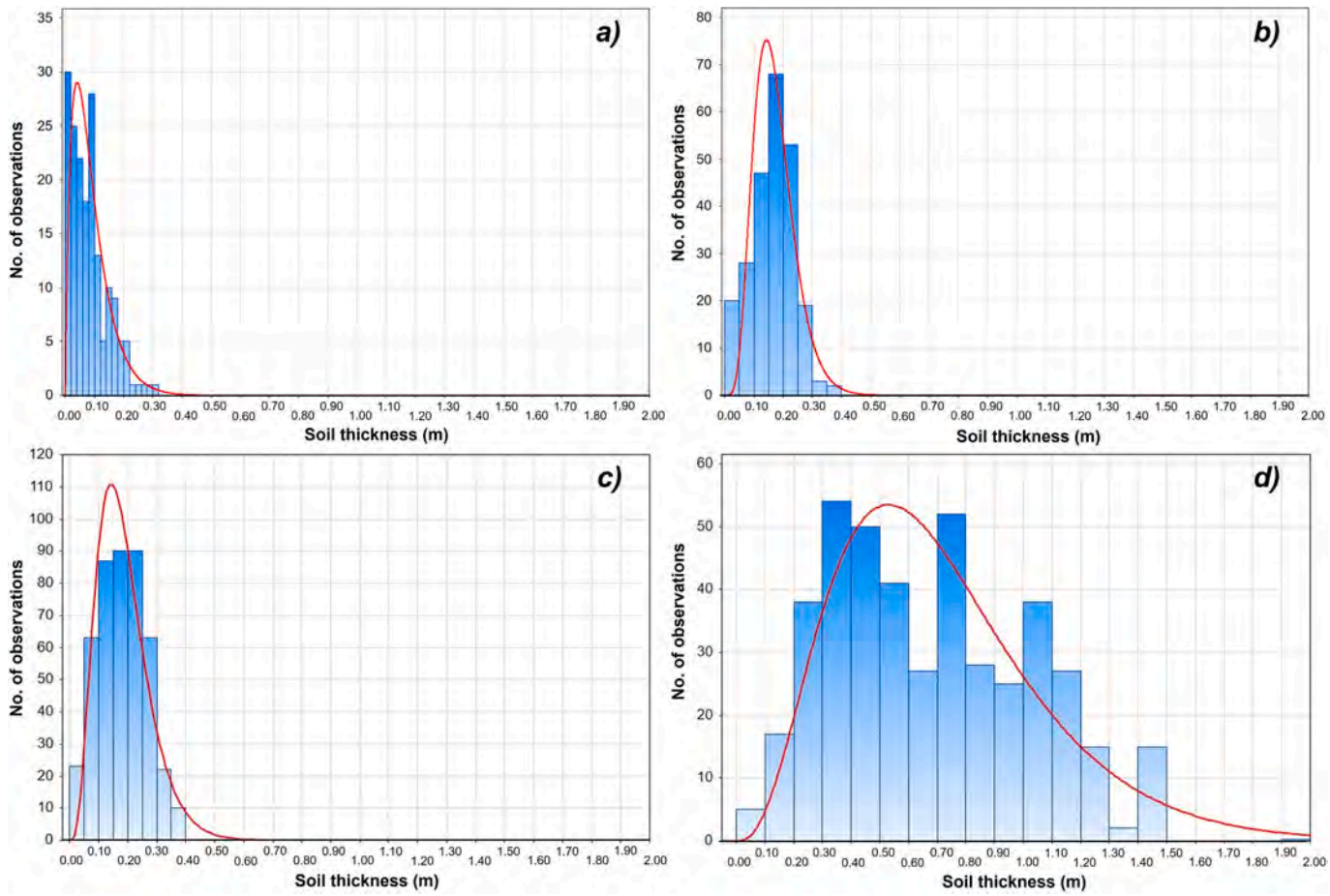

Fig. 5. Gamma probabilistic model applied to soil thickness data for each land cover class. Land cover class a: k = 1.83, θ = 4.71 (Chi-Square test = 27.93020, p = 0.00049); land cover class b: k = 6.21, θ = 2.74 (Chi-square test = 20.83713, p = 0.00011); land cover class c: k = 4.32, θ = 4.31 (Chi-square test = 50.16742, p = 0.00000); land cover class d: k = 3.85, θ = 18.63 (Chi-square test = 76.73999, p = 0.00000).

Moreover, the Annual Groundwater Recharge Coefficient (AGRC, %) proposed for karst aquifers of southern Italy (Allocca et al., 2014) was calculated by using the Eq. (12):

$$AGRC = \frac{[(Qs + Qt) + (Uo - Ui)]}{(P - Er)} \quad (12)$$

where Q_s ($m^3 \cdot s^{-1}$) is the mean annual spring discharge, Q_t ($m^3 \cdot s^{-1}$) is the mean annual tapped discharge by wells, U_o ($m^3 \cdot s^{-1}$) is the mean annual groundwater outflow through adjoining aquifers, and U_i ($m^3 \cdot s^{-1}$) is the mean annual groundwater inflow from adjoining aquifers and allogenic recharge.

4. Results

4.1. Characterization and spatial modeling of the soil mantle

To understand the groundwater recharge processes of the studied karst aquifer, a stratigraphic and thickness characterization of the soil mantle was carried out.

Field observations, including spatial continuity and thickness of the soil mantle as well as vegetation types, allowed the recognition of four land cover classes (Fig. 2): a) denudated areas with prevailing outcropping rocks, erratic and isolated thin soil pockets covered by scarce grassy vegetation; b) denudated areas with sparse outcropping rocks, discontinuous and connected soil pockets and grassy vegetation; c) areas with continuous and thicker soil mantle and grassland; d) areas with the thickest and continuous soil covering and wooded vegetation.

Based on field observations and a supervised classification of Google Earth images, the abovementioned land cover classes were assessed respectively extending over 0.5 % (0.36 km^2) for the class a, 5 % (3.76 km^2) for the class b, 2 % (1.44 km^2) for the class c and 93 % (69.79 km^2) for the class d (Fig. 3).

Measurements of soil thickness were carried out in representative sites of the different land cover classes. Data collected were statistically analyzed resulting with mean values lower for the classes a, b and c, respectively 0.067 m, 0.169 m and 0.167 m and greater values for the class d, with 0.708 m. In addition, to model spatially the soil thickness, data collected for each land cover class were analyzed by a Gamma probabilistic model, whose results were characterized by a high statistical significance showing a probability (p) of the null hypothesis extremely low ($p < 10^{-5}$) for the Chi-Square test (Fig. 5).

Based on results of the probabilistic analysis, a stochastic soil thickness map was reconstructed (Fig. 6i) by considering parameters of the Gamma probabilistic model estimated for each land cover class and the probability value as a random variable Eq. (1).

The validation of the soil thickness map was carried out by field observations and measurements of natural and artificial (road and trail cuts) complete exposures of the soil cover.

4.2. Characterization of physical and index properties of soil mantle

Based on field observations obtained by test pits and observations of the soil profiles, soil mantle belonging to the land covers classes a, b and c were recognized as characterized by the same pedologic soil horizons, even if by different values of the mean thickness and spatial continuity. For this reason, the stratigraphic, physical and hydraulic

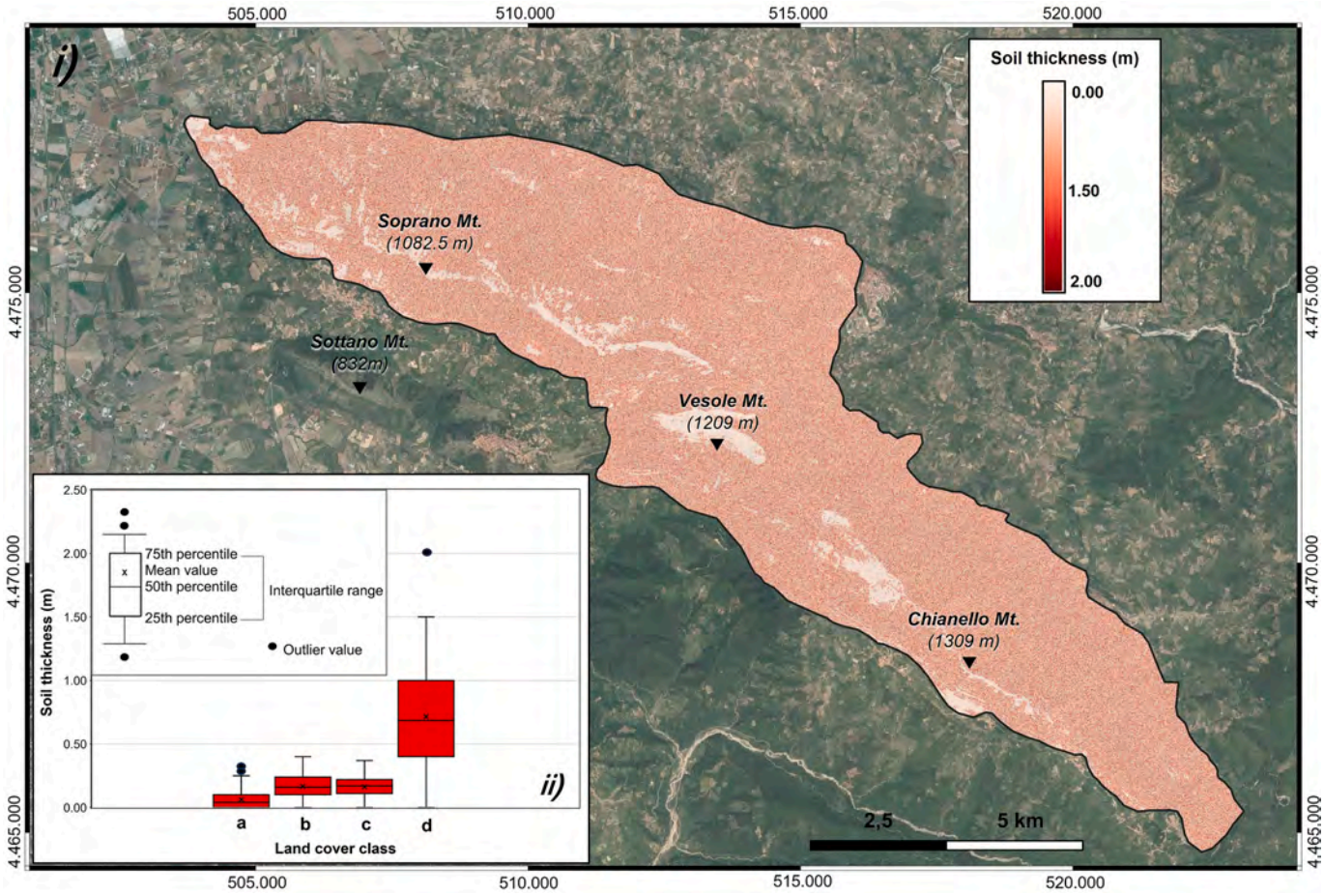

Fig. 6. Stochastic soil thickness map of Soprano-Vesole-Chianello Mts. karst aquifer. Coordinate system UTM WGS 84, 33 N zone; ii) Box plot of soil thickness measured by field surveys in different land cover classes.

characterizations of soils belonging to these land cover classes were related to the only class c, which was considered the most representative of all the three classes. Instead, the characterization of the soil mantle for the land cover class d (wooded areas), were considered independently.

By means of a pit carried out in a site of the Chianello Mt. south-western slope (T.1; Fig. 3), characteristic of the land cover class c, the following pedologic soil horizons were observed from the top to the bottom:

1) A soil horizon (0.10 m thick) characterized by a high content in organic matter (dark brown).
2) B soil horizon (0.22 m thick), classified as ash-fall pyroclastic silty sand (light yellowish brown).

Table 2
Laboratory physical characterization of soil samples and USDA and USCS classifications. Key to symbols: γ_{nat}, natural unit weight; γ_{dry}, dry unit weight; γ_{sat}, saturated unit weight; Gs, unit weight of solid particles; n, porosity; w_L, liquid limit; w_P, plastic limit; PI, plasticity index.

Physical properties	Soil samples			
	Land cover class c	Land cover class d	Land cover class d	Land cover class d
	Sampling depth 0.30 *m*	Sampling depth 0.30 *m*	Sampling depth 0.70 *m*	Sampling depth 1.20 *m*
	I	II	II	III
γ_{nat} (gr·cm^{-3})	0.982	0.932	1.016	1.259
γ_{dry} (gr·cm^{-3})	0.692	0.590	0.616	0.929
γ_{sat} (gr·cm^{-3})	1.411	1.386	1.377	1.584
Index properties	I*	II*	III*	IV*
G_s (gr·cm^{-3})	2.23	2.36	2.47	2.58
n (%)	69.00	74.96	75.04	63.69
w_L (%)	68.58	67.39	75.22	51.66
w_P (%)	61.06	56.97	56.79	46.18
w_R (%)	58.84	39.30	41.56	30.49
PI (%)	7.52	10.42	18.43	15.48
Organic matter (%)	18.48	18.60	19.32	19.01
USDA classification	Sandy Loam	Sandy Loam	Sandy Loam	Sandy Loam
USCS classification	SM	SM	SM	SM

Table 3
Parameters of van Genuchten's equation, obtained for undisturbed soil samples I and II.

Soil samples	I	II
	Land cover class c	Land cover class d
θ_s [−]	0.738	0.788
θ_r [−]	0.001	0.017
α [m^{-1}]	1.985	7.510
n [−]	1.820	1.620

3) R horizon corresponding to the fractured carbonate bedrock with open joints filled by soil derived by the overlying horizon.

By a second pit, executed at Capizzo locality and represetative of the land cover class d (T.2; Fig. 3), the following pedologic soil horizons were recognized:

1) A soil horizon (0.10 m thick), characterized by high organic matters (dark brown color).
2) B soil horizon (0.55 m thick), classified as pyroclastic silty sand (light yellowish brown).
3) Bb soil horizon (0.25 m thick) corresponding to a buried B horizon (paleosol) by subsequent depositional event, and therefore considered as paleosol (dark brownish orange).
4) R horizon corresponding to the fractured carbonate bedrock with open joints filled by soil derived by the overlying soil horizon.

Undisturbed and disturbed soil samples of the B soil horizon were gathered from both pits (T.1 and T.2) while samples of the Bb soil horizon in T.2 only. Physical and index soil properties were determined (Table 2). When the number of soil samples collected for the same sampling depth was greater than one, their mean values were considered.

Among the peculiar features that characterize these soils, the high values of porosity, which varies between 63.7 % and 75.0 % and void ratio, ranging from 1.77 to 3.01 were found. Regarding the Atterberg's limits, values of the liquid limit (w_L) fall between 51.7 % and 75.2 %, while those of the plastic limit (w_P) range between 46.2 % and 61.1 %. As a result, the Plasticity Index (PI) varies from 7.5 % to 18.4 %, thus classifying the soil samples as low plasticity fine sands and silts (ML-OL with PI <50 %). Based on these results, the samples were homogeneously classified as sandy loam, according to USDA classification, and as sand with silt (SM), according to USCS classification.

4.3. Hydraulic characterization of the soil mantle

SWRCs were estimated for two sets of 4 undisturbed soil samples respectively representative of land cover classes c and d (Table 1), for a total number of 8 samples. The undisturbed soil samples belonging to the land cover class d (paleosol) were excluded from this analysis. The hydraulic characterization of paleosol horizon was considered irrelevant for the aim of the research because, based on the results of the soil hydrological monitoring, is excluded from the evapotranspiration processes.

By the comparison of the SWRCs, minor variability in hydraulic soil properties were observed due to different initial soil moisture contents and different grain size distributions. High values of saturated water content (θ_s) were estimated: 73.8 % for the soil samples I (land cover class c); 78.8 % for the soil samples II (land cover class d) (Table 3). Considering the similar unsaturated hydraulic properties of soil horizons investigated, a mean SWRC was considered as representative for soil mantles belonging to the land cover classes c and d (Fig. 7). One SWRC belonging to land cover class c, was excluded due to experimental errors.

Based on the Eq. (4), values of volumetric water content at Field Capacity (θ_{FC}) and Permanent Wilting Point (θ_{PWP}), corresponding to

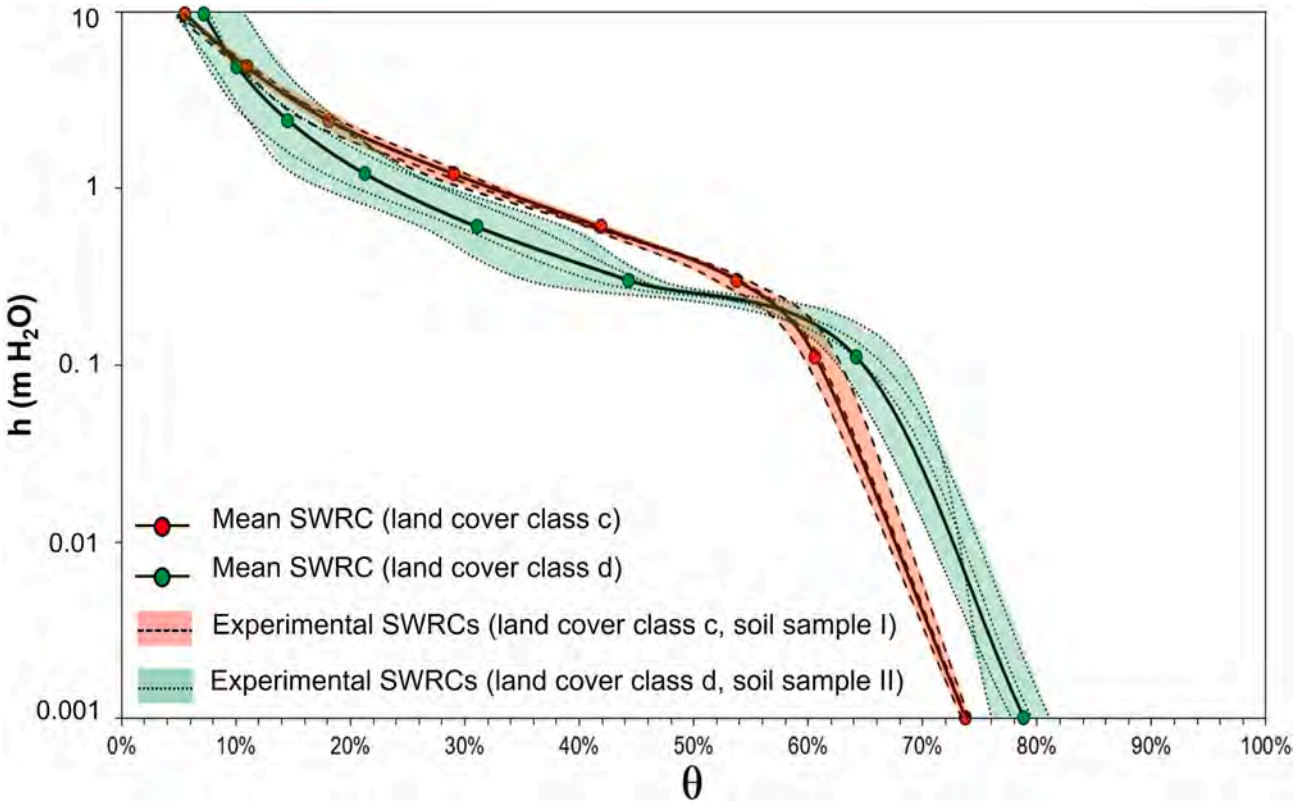

Fig. 7. SWRCs for samples of land cover classes c and d. Mean SWRCs reconstructed by RETC software are represented by continuous thick curves; the dashed curves represent the experimental SWRCs.

Table 4
θ_{FC} and θ_{PWP} estimations for undisturbed soil samples I and II by the application of the van Genuchten model. Estimations of ASWC are also shown.

Soil samples	I	II
	Land cover class c	Land cover class d
θ_{FC} [−]	0.317	0.235
θ_{PWP} [−]	0.006	0.027
ASWC [−]	0.310	0.208
ASWC [%]	31	21

Table 5
K_{sat} values obtained for by the application of the Saxton empirical equation (Eq. (7) to index properties determined on disturbed soil samples.

Soil samples	I*	II*	III*
	Land cover class c	Land cover class d	Land cover class d
K_{sat} ($m \cdot s^{-1}$)	2.18×10^{-4}	4.42×10^{-4}	1.98×10^{-4}

pressure head values of −30 kPa and −1550 kPa (Kirkham, 2005) respectively were calculated as well as their difference (ASWC) for soil mantle of the land cover class c and d (Table 4).

By applying the Eq. (7), K_{sat} values were estimated for soil samples representative of different land cover classes indicating a range varying from 1.98×10^{-4} $m \cdot s^{-1}$ to 4.42×10^{-4} $m \cdot s^{-1}$ (Table 5).

4.4. Soil hydrological monitoring

Results of two representative soil moisture sensors, installed in the land cover classes d (S1) and c (S2), were analyzed. Measured soil moisture showed, for all depths of the soil profiles of the S1 and S2 measuring verticals, a strong rainfall-event and seasonal control with fluctuations varying from hourly to monthly time scales (Fig. 8). The hourly and daily fluctuations of soil water content, directly related to rainfall events, were recognized having an amplitude lesser than the seasonal ones.

During rainy days of the monitoring period, typically occurring from October to March, soil moisture records showed the highest values,

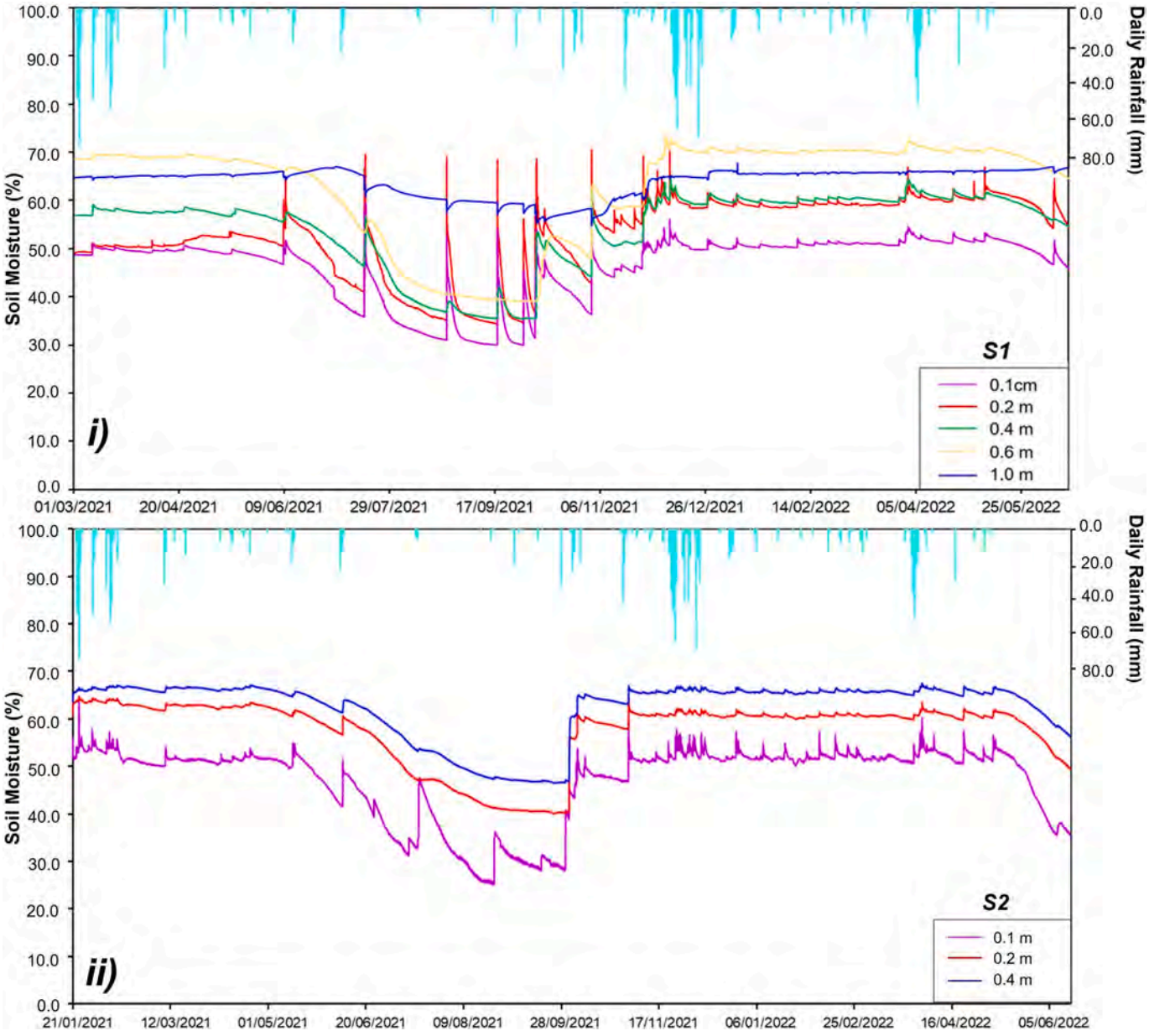

Fig. 8. Measured soil moisture at different depths of representative sites of the land cover classes d (i) and c (ii) during the monitoring period.

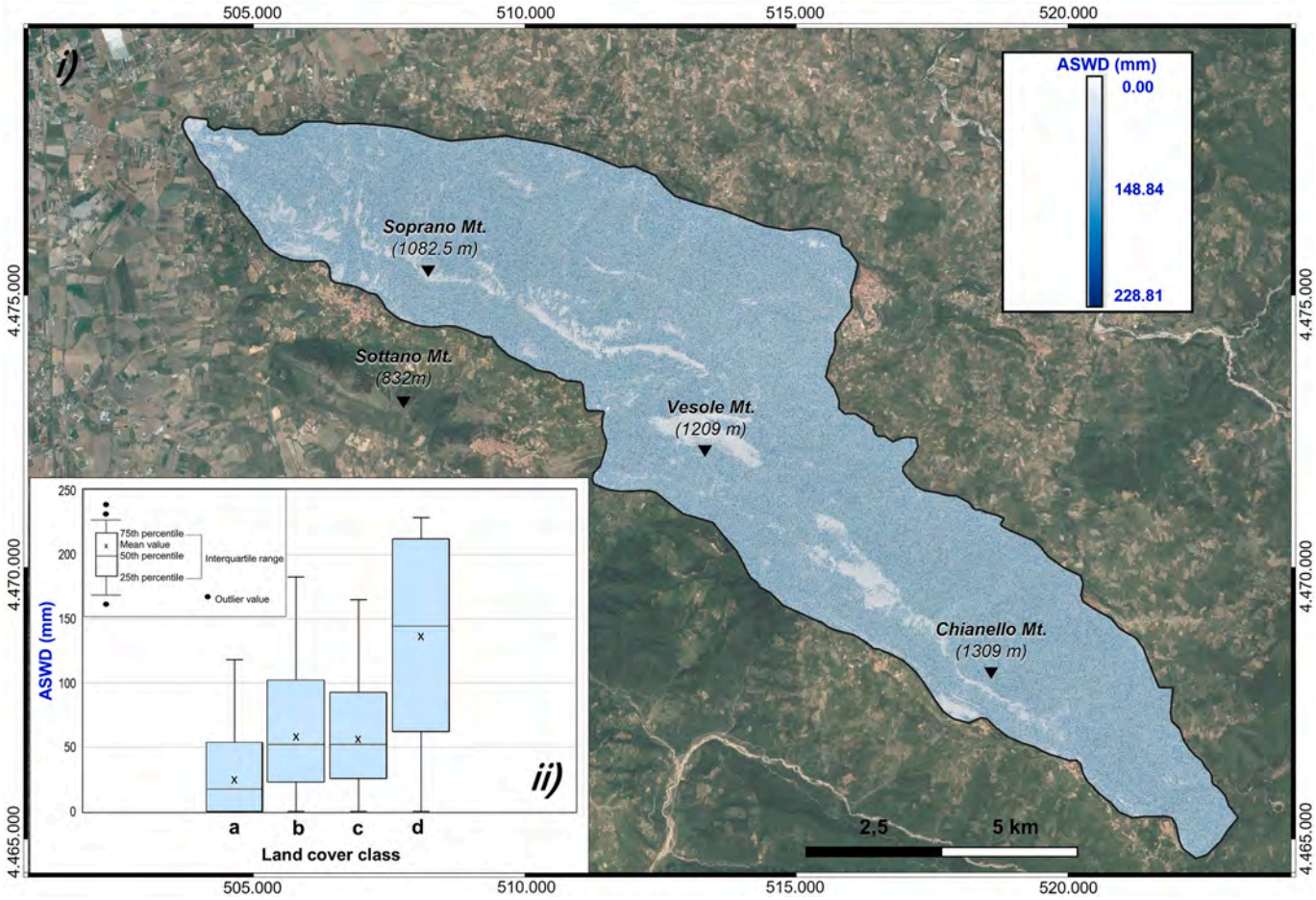

Fig. 9. i) stochastic map of Available Soil Water Depth (ASWD) for the Soprano-Vesole-Chianello Mts. karst aquifer. Coordinate system UTM WGS 84, 33 N zone ii) Box plot of ASWD for different land cover classes.

ranging from 48 % to 68 % and from 52 % to 67 % for S1 and S2 measuring verticals, respectively. During heavy rainfall events with high intensity and duration, fluctuations of soil moisture were observed rapid at lower depths and progressively damped at greater depths. Differently, starting from the late spring until the early autumn, in the period from April to September, a progressive decrease of soil water content was recorded with a higher amplitude and more limited damping effect with depth. For measurement vertical S2, installed in the land cover class c, seasonal fluctuations of soil water content were observed down to the maximum depth explored by sensors (0.40 m) with a limited damping. For the S1 measuring vertical, representative of land cover class d, similar short-term fluctuations of soil water content related to heavy rainfall events were observed as for the S2 measuring vertical. Instead, a progressive decrease of long-term seasonal fluctuations was observed as the depth increases. Considering the linear decreasing trend of seasonal variations of volumetric soil water content with depth, its annulment was estimated at a depth of 1.10 m using a linear regression. Therefore, for the wooded areas (land cover class d), the evapotranspiration zone was considered extended to the maximum depth of 1.10 m. Instead, for other land cover classes (a, b and c), characterized by a thickness lower than 1.10 m, the evapotranspiration zone was considered involving the entire soil profile. Moreover, results of the soil hydrological monitoring led to consider the exclusion from the evapotranspiration zone of the paleosol horizon, which was found at a depth greater than 1.10 m (Table 1).

Based on the elaboration of a stochastic map of soil mantle thickness, for each land cover class, and estimations of Field Capacity (FC) and Permanent Wilting Point (PWP) from the SWRCs, a stochastic map of the Available Soil Water Depth (ASWD) was obtained (Fig. 9i). As a result, the mean values of ASWD, obtained for each land cover classes were estimated in 24.8 mm for class a, 53.6 mm for class b, 52.5 mm for class c and 147.2 mm for class d (Fig. 9ii).

4.5. Soil water balance and estimation of empirical coefficients

The application of the Soil Water Balance code (SWB 1.2) allowed to estimate the spatial distribution of the infiltration and groundwater recharge processes depending on land cover classes.

The spatial variability of groundwater recharge was computed and represented as maps for 2019 and 2020 (Fig. 10) with a mean yearly groundwater recharge value for the studied area resulted in 472.4 $mm \cdot yr^{-1}$ in 2019 and 330.6 $mm \cdot yr^{-1}$ in 2020. Moreover, the components of the water balance, for each land cover classes, were estimated as output of the numerical modeling (Table 6).

Moreover, different evapotranspiration rates were estimated. The highest evapotranspiration values were assessed for the class cover class d, corresponding to an annual rate of 55.7 % and 63.10 % for 2019 and 2020, respectively. Instead, for land cover classes a, b and c, characterized by higher infiltration and groundwater recharge rates, the annual evapotranspiration rate was estimated equal to 36.9 %, 46.6 % and 46.6 %, respectively in 2019, and 38.6 %, 44.7 % e 45.3 %, respectively for 2020. The runoff was estimated as a minor component with values generally lower than 10 % and occurring only during extreme rainfall events. The differences in evapotranspiration were determined by both different values of annual precipitation and the calculation of soil water balance at the daily time scale.

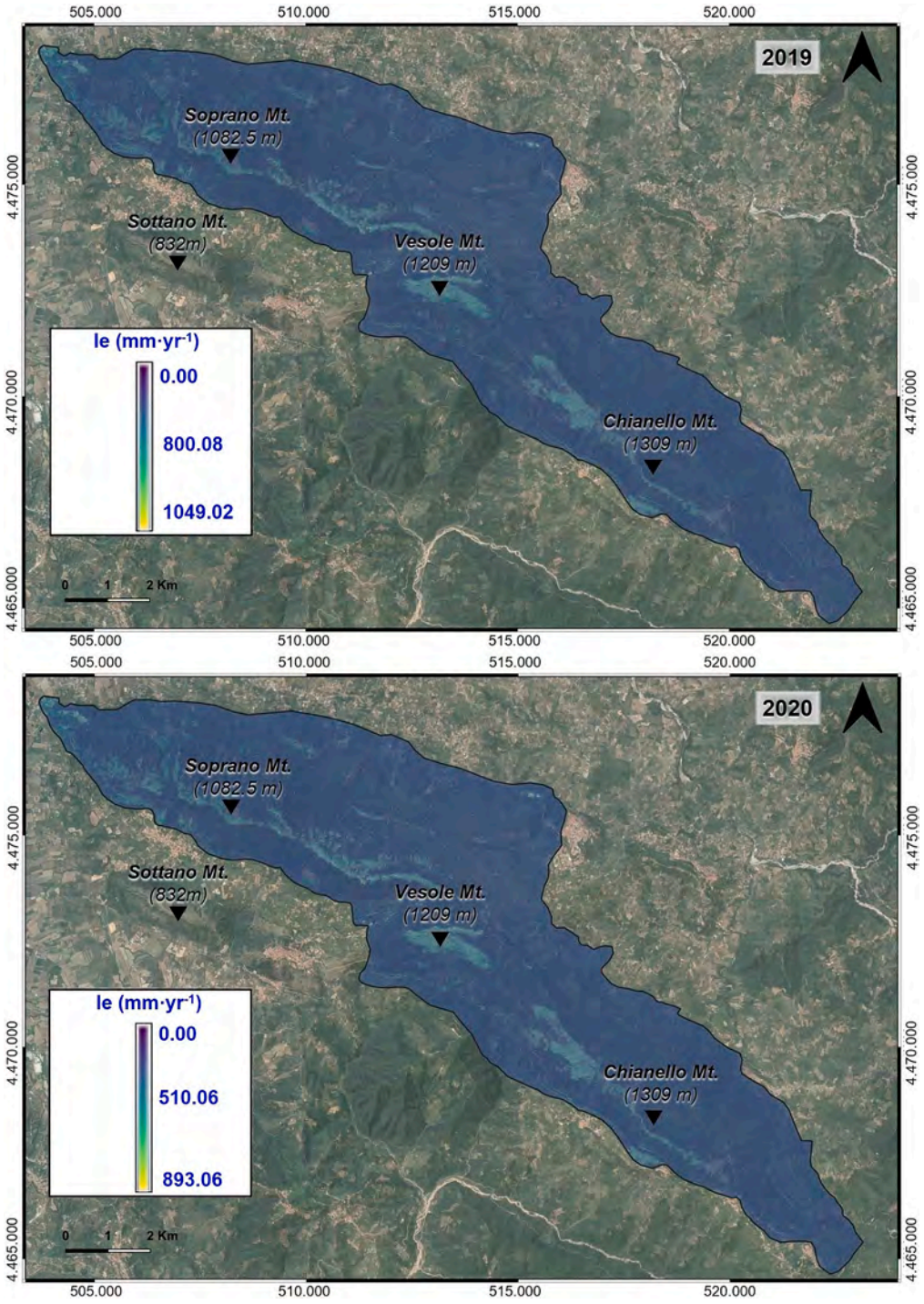

Fig. 10. Groundwater recharge maps obtained by the SWB code for 2019 and 2020. Coordinate system UTM WGS 84, 33 N zone.

Table 6
Components of Soil Water Balance obtained for 2019 and 2020. Keys to symbols: P: Precipitation; Ie: Effective Infiltration; AET: Actual Evapotranspiration; Rs: Surface Runoff.

Land cover class	P (mm·yr^{-1})		Ie (mm·yr^{-1})		AET (mm·yr^{-1})		Rs (mm·yr^{-1})	
	2019	*2020*	*2019*	*2020*	*2019*	*2020*	*2019*	*2020*
a	1102.8	927.2	615.1	482.1	406.5	357.6	81.1	87.4
b			548.8	471.9	517.3	414.5	36.7	41.1
c			548.6	475.5	517.8	420.2	36.4	31.5
d			466.7	324.4	614.5	584.9	20.8	17.9

Table 7
Comparison between annual actual evapotranspiration (AET) rates obtained by SWB code and Thornthwaite-Mater soil water balance.

Land cover class	SWB code AET (%)		Thornthwaite-Mater soil water balance AET (%)	
	2019	*2020*	*2019*	*2020*
a	36.9	38.6	33.9	42.1
b	46.6	44.7	35.5	45.2
c	46.6	45.3	35.4	45.1
d	55.7	63.1	44.0	55.3

The reliability of the results obtained by the SWB code, were also validated by applying the Thornthwaite-Mather empirical approach, in order to mutually compare the results in terms of evapotranspiration rates and trends (Table 7 and Fig. 11). The independent calculations showed in general a good match with a Root Mean Square Error of 15 %, which can be considered due to the daily time scale used by SWB, instead of the monthly one used for the application of the Thornthwaite-Mather method, and to estimation of runoff. Moreover, AET values were found higher for the wooded class (d) than those estimated for the other land cover classes (a, b and c), thus confirming the results of the SWB model.

The temporal variability of soil hydrological processes (evapotranspiration, water surplus and water deficit) were analyzed. When the water stored by soil exceeds the Field Capacity, the infiltration process occurs, generally starting from the wet season (from January to April and from September to December). The dry season (from June to October 2019 and from May to September for 2020) is characterized by a water deficit due to the development of vegetation root system and consequently the increase of evapotranspiration phenomena.

Based on results of SWB model, the Effective Infiltration Coefficient (EIC) and Annual Groundwater Recharge Coefficient (AGRC) were estimated (Table 8) for 2019 and 2020 for each land cover class. Results showed a variability of EIC from 0.42 (class d) to 0.56 (class a), for 2019, while from 0.35 (class d) to 0.52 (class a), for 2020. The high EIC values obtained for denudated areas indicate the infiltration phenomena and then the groundwater recharge as a prevailing component (EIC >50 %). Instead in wooded areas, characterized by lower EIC values, evapotranspiration phenomena represent the predominant one. The obtained values were found in agreement with the coefficients calculated for the European karst aquifers, ranging from 35 % to 76 %, with a mean value around 51 % (Allocca et al., 2014).

Instead, a variability of AGRC from 0.96 (class d) to 0.88 (class a), for 2019, while from 0.95 (class d) to 0.85 (class a), for 2020 were found, in apparent disagreement with previous results (Allocca et al., 2014), which estimated a value equal to 0.62 for the whole Soprano-Vesole-Chianello Mts. karst hydrogeological unit.

5. Discussion

Analyses presented in this work were aimed at the understanding of the hydrological behavior of the coupling soil mantle/land cover type and modeling its effects on groundwater recharge of a representative Mediterranean karst aquifer.

Considering the typical features of karst aquifers of southern Italy, which are discontinuously mantled by ash-fall pyroclastic soil coverings, a quantitative assessment of hydrological processes occurring in this surficial hydrological system and involving the "soil-vegetation-atmosphere system" was considered relevant for advancing the understanding of groundwater processes. This aspect, which concerns the field study of the so-called Earth's Critical Zone (National Research Council, 2001), is usually not analyzed in detail in hydrogeological studies. In addition, several researches considered the vegetation and soil cover, the variation of water content and porosity of soils, as "predictive factors" of the recharge processes of carbonate aquifers (Kim and Jackson, 2012; Scanlon et al., 2005). The methodological approach proposed allowed to advance the knowledge regarding the hydrogeological role of the soil coverings on the recharge processes of the karst aquifer. As novel approach applied to the Soprano-Vesole-Chianello Mts. karst aquifer, representative of other karst aquifers of southern Italy, the field measurements of soil thickness and its stochastic spatial modeling depending on type of land cover were proposed. Moreover, the reconstruction of the stratigraphic settings of soil covering as well as the physical and hydraulic characterization of the soil horizons were also considered.

As a first result, the thickness and stratigraphic settings of soils were found in agreement with the general distribution model of ash-fall pyroclastic deposits along *peri*-Vesuvian slopes (De Vita et al., 2013; Tufano et al., 2021).

A comprehensive characterization of physical properties revealed high values of porosity and void ratio of the soil covering. This is primarily attributed to the abundant interparticle voids, which is typical of volcaniclastic deposits, favoring high values of saturated water content (θ_s >70 %) (De Vita et al., 2013).

Moreover, the texture and/or bulk density properties, which are commonly well-associated with hydraulic properties, were used to apply the Saxton et al. (1986) pedotransfer function and predict the values of saturated hydraulic conductivity (K_{sat}). The resulting high values correspond with measurements of K_{sat} determined for ash-fall pyroclastic soils of the *peri*-vesuvian area (De Vita et al., 2013; De Vita et al., 2018).

The soil hydrological monitoring allowed the recognition of a variability in soil water content from hourly to monthly time scales depending respectively on the effects of single rainfall events and seasonal changes in the evapotranspiration rate.

A similar condition was observed in other studies involving the soil hydrological monitoring in the Mediterranean areas applied to hydrogeological and hydrological studies (Ruiz-Sinoga et al., 2011) and to the assessment of hazard to shallow landsliding (Fusco et al., 2022; Fusco et al., 2017). The sudden increase of water content, induced by extreme rainfall events, indicates a concentrated infiltration in the soil profile, as proposed by Cerdà et al. (1998) and van Schaik et al. (2008). In addition, the field monitoring of water content allowed to identify the lower limit of the root-zone depth favoring the recognition of the evapotranspiration zone for each land cover class, limited to 1.10 m depth for the land cover class d and involving the whole soil covering for the other land cover classes whose thickness is lower. Furthermore, the Available Soil Water Depth (ASWD), within the effective root zone, were calculated by Eq. (6) to apply the soil water balance method.

As results of the Soil Water Balance model (SWB 1.2), high evapotranspiration values were determined for the wooded areas. Instead, for the shallow rooted vegetation, which characterizes the land cover classes a, b and c, groundwater recharge rates higher than the evapotranspiration ones were found (Table 6).

These results can be explained considering the variability of the soil thickness that limit and control the amount of water stored into the soil profile, thus controlling the evapotranspiration process.

Essentially, the land cover class d, characterized by a high thickness of soil affected by the development of deep root-system (>1.00 m), stores the highest values of ASWD, equal to 147.2 mm in average. Instead, the thinner soil mantle of land cover classes a, b and c limits the ASWD to values not exceeding 55 mm, in average. Finally, low runoff rates were estimated and considered negligible. Mean values ranging from 3.9 % for 2019 and 4.8 % for 2020, were quantified for all land cover classes.

The control of thickness of soil covering and the spatial continuity of the soil mantle, as well as the land cover type, on groundwater recharge is the most important and novel result of this study, which advances results of previous researches, showing links between vegetation, climate and soil moisture (Kovačič et al., 2020; Rodriguez-Iturbe et al., 1999). Moreover, results obtained confirm those of other studies which demonstrated that the average annual gross recharge is greater in

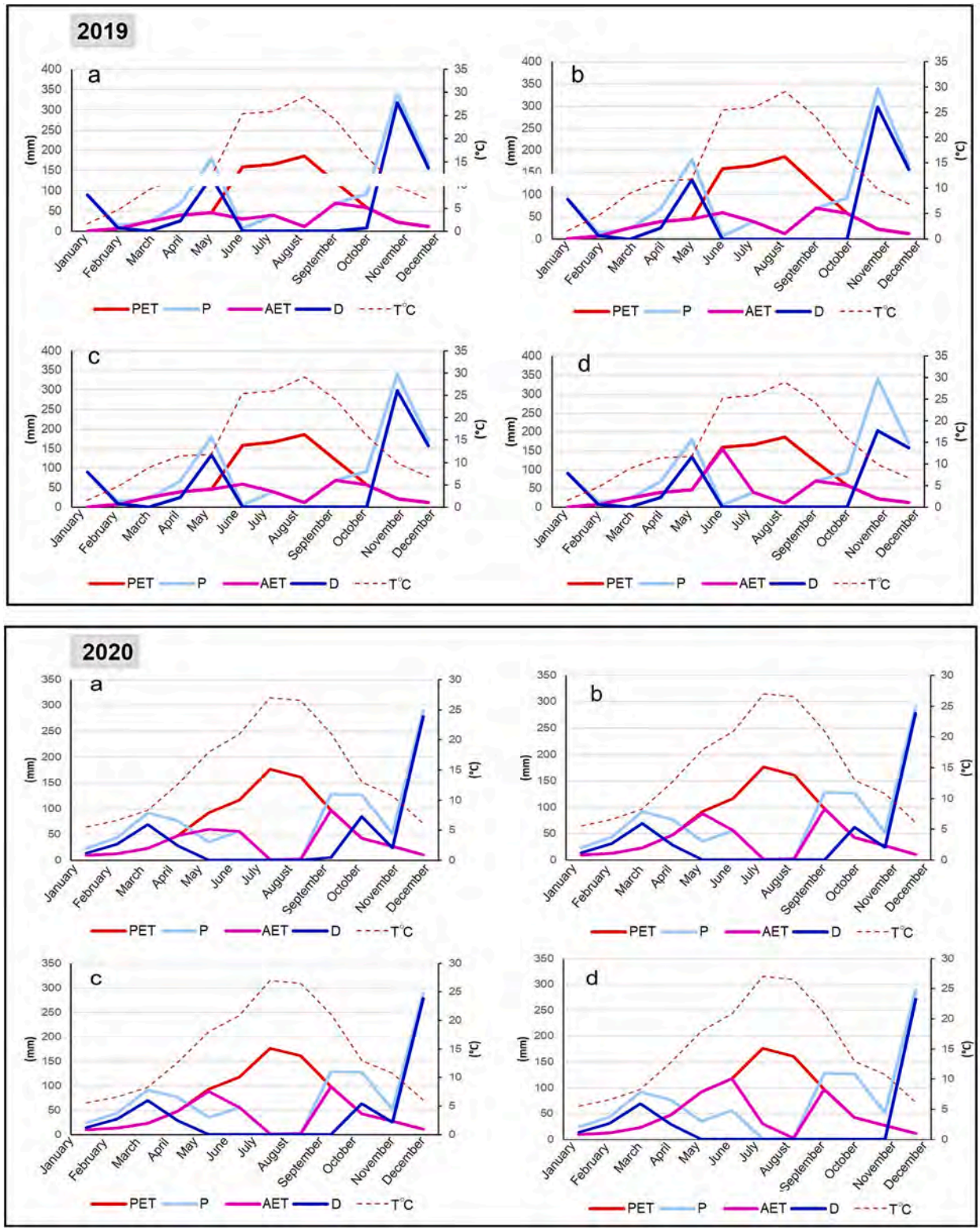

Fig. 11. Monthly soil water balance obtained by the Thornthwaite-Mather method. Key to symbols: P: precipitation (mm); T °(C): air temperature; PET: potential evapotranspiration (mm); AET: actual evapotranspiration (mm); D: water surplus (mm).

grasslands (~52 % of net rainfall) and lower in woodland (~27 % of net infiltration) as results of higher rainfall interception and reduced storage capacity of the vadose zone at forested sites (Fan et al., 2014). Furthermore, these authors suggested that most active roots are developed in the upper 0.60 m for the woodland, in agreement with results showed in the preceding paragraph (par. 4.4). Nosetto et al. (2012) confirmed the greater evapotranspiration rate of the wooded areas, displaying for the wooded sites, values significantly higher than grasslands and areas with herbaceous vegetation cover. This result has been considered arising mainly from a deeper root system and greater direct interception of precipitation, specific features of trees. The results obtained by Zhang and Schilling (2006), are also in agreement with those

Table 8
Effective Infiltration Coefficient (EIC) and Annual Groundwater Recharge Coefficient (AGRC) values obtained for different land cover classes.

Land cover class	EIC		AGRC	
	2019	*2020*	*2019*	*2020*
a	0.56	0.52	0.88	0.85
b	0.50	0.51	0.94	0.94
c	0.50	0.51	0.94	0.94
d	0.42	0.35	0.96	0.95

showed by the present study, recognizing that, given the same soil under different land cover conditions, vegetated soils are characterized by a groundwater recharge lesser than that of bare soils.

In addition, in this work the EIC and AGRC coefficients were also estimated with the aim to assess and compare the effective infiltration. This observation can be related to the difference in effective precipitation values (P-AET), which are equal to 588.7 mm for 2019, and to 482.9 mm for 2020 on average, instead estimated equal to 1225 mm in Allocca et al. (2014) by a regional empirical correlation with the altitude. Finally, in the present work, only two consecutive hydrologic years (2019–2020) were considered, unlike Allocca et al. (2014), which analyzed P –AET as mean annual value over the period 1926 – 2012.

The approaches and results proposed in this work are conceived to be exportable also to other karst aquifers of the Mediterranean area due to the volcanism occurred during Pleistocene in other volcanic provinces, as for the cases of karst aquifers of Greece, Turkey and Lebanon. In particular, the Eastern Mediterranean region was characterized by a high frequency and intensity of explosive volcanic eruptions, e.g. Santorini, Kos, in the Aegean sea (Bruins et al., 2008), Isparta- Gölcük, Erciye and Süphan in Anatolia (Deniel et al., 1998), with widespread dispersal of ash-fall pyroclastic soils, which result in significant pyroclastic series with different chemical composition (Hamann et al., 2010; Polacci et al., 2003; Zanchetta et al., 2011).

6. Conclusions

The methodological approaches proposed in this work offer a study procedure for the recognition and estimation of the hydrological control of soil mantle and land cover types on groundwater recharge. The results achieved are considered particularly significant, especially for having recognized the relevance of the coupling soil thickness/land cover type on the Available Soil Water Depth and evapotranspiration rate, both controlling the groundwater recharge. Consequently, results obtained allow recognizing soil mantle as a complex hydrological system which plays a non-negligible role in the groundwater recharge process. Moreover, the results obtained represent an improvement in the field of the hydrogeological knowledge which, for most of the karst aquifers of the southern Apennines, appears still being general and not suitable for the application of advanced models aimed at the estimation of effects of climate change scenarios.

The integrated use of field, laboratory and modeling approaches represents a valid tool for the estimation and modeling, at basin scale, of groundwater recharge processes allowing a more accurate quantification of hydrogeological parameters influencing the groundwater recharge.

The obtained results might also be used by regional planners and stakeholders to assess the potential impacts of urbanization, land-use and climate changes on patterns and rates of groundwater recharge as well. The method proposed is conceived as being exportable to other karst aquifers of southern Italy and of the world, in all cases in which soil mantle exerts a relevant role on hydrological regime and groundwater recharge.

CRediT authorship contribution statement

Delia Cusano: Conceptualization, Data curation, Formal analysis, Investigation, Methodology, Software, Validation, Writing – original draft, Writing – review & editing. **Daniele Lepore:** . **Vincenzo Allocca:** Conceptualization, Data curation, Formal analysis, Writing – review & editing. **Pantaleone De Vita:** Conceptualization, Data curation, Formal analysis, Funding acquisition, Investigation, Methodology, Project administration, Resources, Software, Supervision, Validation, Writing – original draft, Writing – review & editing.

Declaration of competing interest

The authors declare that they have no known competing financial interests or personal relationships that could have appeared to influence the work reported in this paper.

Data availability

Data will be made available on request.

Acknowledgements

Authors acknowledge the funding of the research by MedWater project (http://grow-medwater.de/home/) promoted by the German Federal Ministry of Education and Research (BMFB) and aimed at the assessment of groundwater of karst aquifers of Mediterranean areas and the PhD Program of Dipartimento di Scienze della Terra, dell'Ambiente e delle Risorse (DiSTAR), Università di Napoli Federico II (34th cycle). The authors would also like to thank the President of the Province of Salerno Francesco Alfieri for leading the agreement stipulated in May 2019 between the Department of Earth, Environmental and Resource Sciences (DiSTAR), University of Naples Federico II, and the Municipalities of Capaccio Paestum, Giungano, Monteforte Cilento, Roccadaspide and Trentinara, which was aimed at logistically supporting the research activity.

References

Allocca, V., Manna, F., De Vita, P., 2014. Estimating annual groundwater recharge coefficient for karst aquifers of the southern Apennines (Italy). Hydrology and Earth System Sciences 18, 803–817. https://doi.org/10.5194/hess-18-803-2014.

ASTM D421-85, 1998. Practice for dry preparation of soil samples for particle-size analysis and determination of soil constant. Annual Book of American Society for Testing and Material Standards, West Conshohocken, USA.

ASTM D422-63, 1998. Standard test method for particle-size analysis of soils, Annual Book of American Society for Testing and Material Standards, West Conshohocken, USA.

ASTM D4318, 1984. Standard test method for liquid limit, plastic limit and plasticity idex of soil, Annual Books of ASTM Standards.

ASTM D854-83, 1983. Standard Test Methods for Specific Gravity of Soil Solids by Water Picnometer.

ASTM-D2974, 2000. Standard Test Methods for Moisture, Ash, and Organic Matter of Peat and Other Organic Soils, ASTM International.

Bakalowicz, M., 2005. Karst groundwater: a challenge for new resources. Hydrogeol J 13, 148–160. https://doi.org/10.1007/s10040-004-0402-9.

Beck, H.E., Zimmermann, N.E., McVicar, T.R., Vergopolan, N., Berg, A., Wood, E.F., 2018. Present and future Köppen-Geiger climate classification maps at 1-km resolution. Sci Data 5, 180214. https://doi.org/10.1038/sdata.2018.214.

Bisson, M., Pareschi, M.T., Zanchetta, G., Sulpizio, R., Sanatacroce, R., 2007. Volcaniclastic 692 debris-flow occurrences in the Campania region (Southern Italy) and their relation to 693 Holocene-Late Pleistocene pyroclastic fall deposits: implications for large-scale hazard 694 mapping. Bulletin of Volcanology 70, 157–167. https://doi.org/10.1007/s00445-007-0127- 695 4.

Bonacci, O., 2001. Montly and annual effective infiltration coefficients in Dinaric karst: example of the Gradole karst spring catchment. Hydrological Sciences - Journal Des Sciences Hydrologiques 46 (2). https://doi.org/10.1080/02626660109492822.

Borzì, I., Bonaccorso, B., Aronica, G.T., 2020. The Role of DEM Resolution and Evapotranspiration Assessment in Modeling Groundwater Resources Estimation: A Case Study in Sicily. Water 12, 2980. https://doi.org/10.3390/w12112980.

Bouma, J., 1989. Using Soil Survey Data for Quantitative Land Evaluation. Using Soil Survey Data for Quantitative. Land Evaluation 9, 177–213.

British Standard (BS) 1377, 1990. Methods of test for Soils for civil engineering purposes.

Bruins, H.J., MacGillivray, J.A., Synolakis, C.E., Benjamini, C., Keller, J., Kisch, H.J., Klügel, A., Van Der Plicht, J., 2008. Geoarchaeological tsunami deposits at Palaikastro (Crete) and the Late Minoan IA eruption of Santorini. Journal of Archaeological Science 35, 191–212. https://doi.org/10.1016/j.jas.2007.08.017.
Casagrande A., 1948. Classification and Identification of Soils, Transactions, ASCE.
Celico, P.B., 1983. Idrogeologia dei massicci carbonatici, delle piane quaternarie e delle aree vulcaniche dell' Italia centro-meridionale (Marche e Lazio meridionali, Abruzzo, Molise e Campania). Cassa per Il Mezzogiorno 4 (2), 1–225.
Celico, P., Guadagno, F.M., 1998. L'instabilità delle coltri piroclastiche delle dorsali 718 carbonatiche in Campania: attuali conoscenze. Quaderni Di Geologia Applicata 5 (1), 129, 719 188.
Cerdà, A., Schnabel, S., Ceballos, A., Gomez-Amelia, D., 1998. Soil hydrological response under simulated rainfall in the Dehesa land system (Extremadura, SW Spain) under drought conditions. Earth Surface Processes and Landforms 23, 195–209.
Charlier, J.-B., Bertrand, C., Mudry, J., 2012. Conceptual hydrogeological model of flow and transport of dissolved organic carbon in a small Jura karst system. Journal of Hydrology 460–461, 52–64. https://doi.org/10.1016/j.jhydrol.2012.06.043.
Christensen, J.H., Hewitson, B., Busuioc, A., Chen, A., Gao, X., Held, I., Jones, R., Kolli, R.K., Kwon, W.T., Laprise, R., Magana Rueda, V., Mearns, L., Mearns, C.G., Raisanen, J., Rinke, A., Sarr, A., Whetton, P., 2007. Regional Climate Projections 11, 847–940. Available at http://www.ipcc.ch/pdf/assessment-report/ar4/wg1/ar4-wg1-chapter11.pdf.
Congedo L., 2016. Semi-Automatic Classification Plugin Documentation.
Cronshey, R., 1986. Urban hydrology for small watersheds, 55. US Department of Agriculture, Soil Conservation Service, Engineering Division.
Cusano, D., Allocca, V., Fusco, F., Tufano, R., De Vita, P., 2019. Multi-scale assessment of groundwater vulnerability to pollution: study cases from Campania region (Southern Italy). Italian Journal of Engineering Geology and Environment 19-24. https://doi.org/10.4408/IJEGE.2019-01.S-03.
De Vita, P., Napolitano, E., Godt, J.W., Baum, R.L., 2013. Deterministic estimation of hydrological thresholds for shallow landslide initiation and slope stability models: case study from the Somma-Vesuvius area of southern Italy. Landslides 10, 713–728. https://doi.org/10.1007/s10346-012-0348-2.
De Vita, P., Allocca, V., Celico, F., Fabbrocino, S., Cesaria, M., Monacelli, G., Musilli, I., Piscopo, V., Scalise, A.R., Summa, G., Tranfaglia, G., Celico, P., 2018. Hydrogeology of continental southern Italy. Hydrogeology of Continental Southern Italy, JOURNAL OF MAPS 14, 230–241. https://doi.org/10.1080/17445647.2018.1454352.
Del Soldato, M., Pazzi, V., Segoni, S., De Vita, P., Tofani, V., Moretti, S., 2018. Spatial modeling of pyroclastic cover deposit thickness (depth to bedrock) in peri-volcanic areas of Campania (southern Italy). Earth Surface Processes and Landforms 43, 1757–1767. https://doi.org/10.1002/esp.4350.
Deniel, C., Aydar, E., Gourgaud, A., 1998. The Hasan Dagi stratovolcano žCentral Anatolia, Turkey/ : evolution from calc-alkaline to alkaline magmatism in a collision zone.
Drogue, C., 1971. Coefficient d'infiltration ou infiltration efficace, sur les roches calcaires. Actes Colloque D'hydrologie En Pays Calcaire, Besançon 121–131.
Fan, J., Oestergaard, K.T., Guyot, A., Lockington, D.A., 2014. Estimating groundwater recharge and evapotranspiration from water table fluctuations under three vegetation covers in a coastal sandy aquifer of subtropical Australia. Journal of Hydrology 519, 1120–1129. https://doi.org/10.1016/j.jhydrol.2014.08.039.
Fu, Z., Chen, H., Xu, Q., Jia, J., Wang, S., Wang, K., 2016. Role of epikarst in near-surface hydrological processes in a soil mantled subtropical dolomite karst slope: implications of field rainfall simulation experiments. Hydrological Processes 30, 795–811. https://doi.org/10.1002/hyp.10650.
Fusco, F., Allocca, V., De Vita, P., 2017. Hydro-geomorphological modelling of ash-fall pyroclastic soils for debris flow initiation and groundwater recharge in Campania (southern Italy). CATENA 158, 235–249. https://doi.org/10.1016/j.catena.2017.07.010.
Fusco, F., Bordoni, M., Tufano, R., Vivaldi, V., Meisina, C., Valentino, R., Bittelli, M., De Vita, P., 2022. Hydrological regimes in different slope environments and implications on rainfall thresholds triggering shallow landslides. Nat Hazards 114, 907–939. https://doi.org/10.1007/s11069-022-05417-5.
Goldscheider, N., 2015. Overview of Methods Applied in Karst Hydrogeology. In: Stevanović, Z. (Ed.), Karst Aquifers—Characterization and Engineering, Professional Practice in Earth Sciences. Springer International Publishing, Cham, pp. 127–145. https://doi.org/10.1007/978-3-319-12850-4_4.
Hamann, Y., Wulf, S., Ersoy, O., Ehrmann, W., Aydar, E., Schmiedl, G., 2010. First evidence of a distal early Holocene ash layer in Eastern Mediterranean deep-sea sediments derived from the anatolian volcanic province. Quaternary Research 73, 497–506. https://doi.org/10.1016/j.yqres.2009.12.004.
Hartmann, A., Goldscheider, N., Wagener, T., Lange, J., Weiler, M., 2014. Karst water resources in a changing world: Review of hydrological modeling approaches: KARST WATER RESOURCES PREDICTION. Rev. Geophys. 52, 218–242. https://doi.org/10.1002/2013RG000443.
Jukić, D., Denić-Jukić, V., Lozić, A., 2021. An alternative method for groundwater recharge estimation in karst. Journal of Hydrology 600, 126671. https://doi.org/10.1016/j.jhydrol.2021.126671.
Kim, J.H., Jackson, R.B., 2012. A Global Analysis of Groundwater Recharge for Vegetation, Climate, and Soils. Vadose Zone Journal 11 (1). https://doi.org/10.2136/vzj2011.0021RA.
Kirkham, M.B., 2005. Principles of soil and plant water relations. Elsevier Academic Press, Amsterdam, New York.
Kovačič, G., Petrič, M., Ravbar, N., 2020. Evaluation and Quantification of the Effects of Climate and Vegetation Cover Change on Karst Water Sources: Case Studies of Two Springs in South-Western Slovenia. Water 12, 3087. https://doi.org/10.3390/w12113087.
Mao, D., Cherkauer, K.A., 2009. Impacts of land-use change on hydrologic responses in the Great Lakes region. Journal of Hydrology 374, 71–82. https://doi.org/10.1016/j.jhydrol.2009.06.016.
Matheussen, B., Kirschbaum, R.L., Goodman, I.A., O'Donnell, G.M., Lettenmaier, D.P., 2000. Effects of land cover change on streamflow in the interior Columbia River Basin (USA and Canada). Hydrological Processes 14, 867–885. https://doi.org/10.1002/(SICI)1099-1085(20000415)14:5<867::AID-HYP975>3.0.CO;2-5.
National Research Council, 2001. Preparing for an Aging World: The Case for Cross-National Research. https://doi.org/doi:10.17226/10120.
Nosetto, M.D., Jobbágy, E.G., Brizuela, A.B., Jackson, R.B., 2012. The hydrologic consequences of land cover change in central Argentina. Agriculture, Ecosystems & Environment 154, 2–11. https://doi.org/10.1016/j.agee.2011.01.008.
Pinto, C.A., Nadezhdina, N., David, J.S., Kurz-Besson, C., Caldeira, M.C., Henriques, M. O., Monteiro, F.G., Pereira, J.S., David, T.S., 2014. Transpiration in Quercus suber trees under shallow water table conditions: the role of soil and groundwater. Hydrological Processes 28, 6067–6079. https://doi.org/10.1002/hyp.10097.
Polacci, M., Pioli, L., Rosi, M., 2003. The Plinian phase of the Campanian Ignimbrite eruption (Phlegrean Fields, Italy): evidence from density measurements and textural characterization of pumice. Bull Volcanol 65, 418–432. https://doi.org/10.1007/s00445-002-0268-4.
Polemio, M., Casarano, D., 2008. Climate change, drought and groundwater availability in southern Italy. Climate Change, Drought and Groundwater Availability in Southern Italy, Geological Society, London, Special Publications 288, 39–51. https://doi.org/10.1144/SP288.4.
Rodriguez-Iturbe, I., Porporato, A., Ridolfi, L., Isham, V., Coxi, D.R., 1999. Probabilistic modelling of water balance at a point: the role of climate, soil and vegetation. Proc. r. Soc. Lond. A 455, 3789–3805. https://doi.org/10.1098/rspa.1999.0477.
Ruggieri, G., Allocca, V., Borfecchia, F., Cusano, D., Marsiglia, P., De Vita, P., 2021. Testing Evapotranspiration Estimates Based on MODIS Satellite Data in the Assessment of the Groundwater Recharge of Karst Aquifers in Southern Italy. Water 13, 118. https://doi.org/10.3390/w13020118.
Ruiz-Sinoga, J.D., Martínez-Murillo, J.F., Gabarrón-Galeote, M.A., García-Marín, R., 2011. The effects of soil moisture variability on the vegetation pattern in Mediterranean abandoned fields (Southern Spain). CATENA 85, 1–11. https://doi.org/10.1016/j.catena.2010.11.004.
Santoro, M., 1970. Sulla applicabilita della formula di Turc per il calcolo della evapotraspirazione effettiva in Sicilia. Proceedings I International Conference on Groundwater, I. A. H., Palermo.
Saxton, K.E., Rawls, W.J., Romberger, J.S., Papendick, R.I., 1986. Estimating Generalized Soil-water Characteristics from Texture. Soil Science Society of America Journa 50, 1031–1036. https://doi.org/10.2136/sssaj1986.03615995005000040039x.
Scanlon, B.R., Healy, R.W., Cook, P.G., 2002. Choosing appropriate techniques for quantifying groundwater recharge. Hydrogeology Journal 10, 18–39. https://doi.org/10.1007/s10040-001-0176-2.
Scanlon, B.R., Reedy, R.C., Stonestrom, D.A., Prudic, D.E., Dennehy, K.F., 2005. Impact of land use and land cover change on groundwater recharge and quality in the southwestern US. Global Change Biology 11, 1577–1593. https://doi.org/10.1111/j.1365-2486.2005.01026.x.
Simone, L., Bravi, S., Carannante, G., Masucci, I., Pomoni-Papaioannou, F., 2012. Arid versus wet climatic evidence in the "middle Cretaceous" calcareous successions of the Southern Apennines (Italy). Cretaceous Research 36, 6–23. https://doi.org/10.1016/j.cretres.2012.01.005.
Srebrenović, D., 1986. Primijenjana hidrologija (Applied Hydrology). Tehnička knjiga Zagreb, Yugoslavia.
Thornthwaite, C.W., 1955. The Water Balance. Climatol. 8 (1), 1–104.
Thornthwaite, C.W., Mather, J.R., 1957. Instructions and tables for computing potential evapotranspiration and the water balance. Centerton, New Jersey Laboratory of Climatology, Publications in Climatology 10 (3), 185–311.
Torrente, M.M., Civile, D., Martino, C., Milia, A., 2000. Assetto strutturale ed evoluzione tettonica dell'area di Monte Vesole-Monte Chianello (Cilento, Appennino meridionale). Italian Journal of Geosciences 119 (3), 733–747.
Trček, B., 2007. How can the epikarst zone influence the karst aquifer hydraulic behaviour? Environ Geol 51, 761–765. https://doi.org/10.1007/s00254-006-0387-x.
Tufano, R., Allocca, V., Coda, S., Cusano, D., Fusco, F., Nicodemo, F., Pizzolante, A., De Vita, P., 2020. Groundwater vulnerability of principal aquifers of the Campania region (southern Italy). Journal of Maps 16 (2), 565–576. https://doi.org/10.1080/17445647.2020.1787887.
Tufano, R., Formetta, G., Calcaterra, D., De Vita, P., 2021. Hydrological control of soil thickness spatial variability on the initiation of rainfall-induced shallow landslides using a three-dimensional model. Landslides 18, 3367–3380. https://doi.org/10.1007/s10346-021-01681-x.
Turc, L., 1954. e bilan d'eau des sols: Relation entre la precipitations, l'evaporation et l'ecoulement. Annales Agronomiques 5, 491.
USDA, 1987. Soil mechanics level I. module 3 – USDA textural soil classification study guide. National Employee Development Staff, Soil Conservation Service, United States Department of Agriculture, Government Printing Office, Washington, DC, U.S.
van Genuchten, M.T., 1980. A closed form equation for predicting the hydraulic conductivity of unsaturated soils. Soil Science Society of America Journal 44, 892–898. https://doi.org/10.2136/sssaj1980.03615995004400050002x.
van Genuchten, M.T., Leij, F.J., Jates, S.R., 1991. The Retc code for quantifying the hydraulic functions of unsaturated soils. T U.S. Department of Agriculture, Agricultural Research Service, Report IAG-DW12933934, Riverside, CA EPA/600, 2–91.

van Schaik, N.L.M.B., Schnabel, S., Jetten, V.G., 2008. The influence of preferential flow on hillslope hydrology in a semi-arid watershed (in the Spanish Dehesas). Hydrological Processes 22, 3844–3855. https://doi.org/10.1002/hyp.6998.

Verma, S., Verma, R.K., Mishra, S.K., Singh, A., Jayaraj, G.K., 2017. A revisit of NRCS-CN inspired models coupled with RS and GIS for runoff estimation. Hydrological Sciences Journal 62, 1891–1930. https://doi.org/10.1080/02626667.2017.1334166.

Vitale, S., Dati, F., Mazzoli, S., Ciarcia, S., Guerriero, V., Iannace, A., 2012. Modes and timing of fracture network development in poly-deformed carbonate reservoir analogues, Mt. Chianello, southern Italy. Journal of Structural Geology 37, 223–235. https://doi.org/10.1016/j.jsg.2012.01.005.

Westenbroek, S., Kelson, V.A., Dripps, W.R., Hunt, R.J., Bradbury, K.R., 2010. SWB–a modified Thornthwaite-Mather Soil-Water-Balance Code for estimating groundwater recharge, Techniques and Methods. US Department of the Interior, US Geological Survey, Ground Resources Program, Reston, VA, USA.

Zanchetta, G., Sulpizio, R., Roberts, N., Cioni, R., Eastwood, W.J., Siani, G., Caron, B., Paterne, M., Santacroce, R., 2011. Tephrostratigraphy, chronology and climatic events of the Mediterranean basin during the Holocene: An overview. The Holocene 21 (1), 33–52. https://doi.org/10.1177/0959683610377531.

Zhang, Y.-K., Schilling, K.E., 2006. Effects of land cover on water table, soil moisture, evapotranspiration, and groundwater recharge: A Field observation and analysis. Journal of Hydrology 319, 328–338. https://doi.org/10.1016/j.jhydrol.2005.06.044.

Zhang, J., Zhou, L., Ma, R., Jia, Y., Yang, F., Zhou, H., Cao, X., 2019. Influence of soil moisture content and soil and water conservation measures on time to runoff initiation under different rainfall intensities. CATENA 182, 104172. https://doi.org/10.1016/j.catena.2019.104172.

Žugaj, R., 1995. Regionalna hidrološka analiza u kršu Hrvatske (Regional Hydrological Analysis in Croatian Karst). Croatian Hydrological Society, Zagreb.